

1                    **A MULTI-FACETED STUDY OF NEMATIC ORDER**  
2                    **RECONSTRUCTION IN MICROFLUIDIC CHANNELS.\***

3                    JAMES DALBY<sup>†</sup>, YUCEN HAN<sup>†</sup>, APALA MAJUMDAR<sup>\*†</sup>, AND LIDIA MRAD<sup>‡</sup>

4                    **Abstract.** We study order reconstruction (OR) solutions in the Beris-Edwards framework for  
5                    nematodynamics, for both passive and active nematic flows in a microfluidic channel. OR solutions  
6                    exhibit polydomains and domain walls, and as such, are of physical interest. We show that OR  
7                    solutions exist for passive flows with constant velocity and pressure, but only for specific boundary  
8                    conditions. We prove the existence of unique, symmetric and non-singular nematic profiles, for  
9                    boundary conditions that do not allow for OR solutions. We compute asymptotic expansions for  
10                    OR-type solutions for passive flows with non-constant velocity and pressure, and active flows, which  
11                    shed light on the internal structure of domain walls. The asymptotics are complemented by numerical  
12                    studies that demonstrate the universality of OR-type structures in static and dynamic scenarios.

13                    **Key words.** Nematodynamics, Active liquid crystals, Microfluidics

14                    **AMS subject classifications.** 34A34 , 34E10, 76A15

15                    **1. Introduction.** Nematic liquid crystals (NLCs) are mesophases that combine  
16                    fluidity with the directionality of solids [13]. The NLC molecules tend to align along  
17                    certain locally preferred directions, leading to a degree of long-range orientational  
18                    order. The orientational ordering results in direction-dependent physical properties  
19                    that render them suitable for a range of industrial applications, including optical  
20                    displays. When confined to thin planar cells and in the presence of fluid flow, applica-  
21                    tions of nematics are further extended, for example, to optofluidic devices and guided  
22                    micro-cargo transport through microfluidic networks [11, 35]. These hydrodynamic  
23                    applications are facilitated by the coupling between the fluidity and the orientational  
24                    ordering, leading to exceptional mechanical and rheological properties [31].

25                    Flow-induced deformation of nematic textures in confinement are ubiquitous, both  
26                    in passive systems where the hydrodynamics are driven by external agents, as well  
27                    as in active systems. Active matter systems, composed of self-driven units, also  
28                    exhibit orientational ordering and collective motion, resulting in a wealth of intriguing  
29                    non-equilibrium properties [30]. We focus on passive and active nematodynamics in  
30                    microfluidic channels, with a view to model spatio-temporal pattern formation and  
31                    to analyse the stability of singular lines or domain walls in such channels.

32                    We work with long, shallow, three-dimensional (3D) microfluidic channels of  
33                    width  $L$ , in a reduced Beris-Edwards framework [4]. Our domain is effectively one-  
34                    dimensional (1D), since we assume that structural details are invariant across the  
35                    length and height of the channel. We work with a reduced Landau-de Gennes (LdG)  
36                    **Q**-tensor for the nematic ordering. This reduced **Q**-tensor has two degrees of freedom  
37                    - the planar nematic director,  $\mathbf{n}$ , in the two-dimensional (2D) channel cross-section,  
38                    and an order parameter,  $s$ , related to the degree of nematic ordering. The director  $\mathbf{n}$

---

\*Submitted to the editors DATE.

**Funding:** AM is supported by the University of Strathclyde New Professors Fund, a Leverhulme International Academic Fellowship, an OCIAM Visiting Fellowship at the University of Oxford and a Daiwa Foundation Small Grant. JD acknowledges support from the University of Strathclyde and the DST-UKIERI. YH is supported by a Royal Society Newton International Fellowship.

<sup>†</sup>Department of Mathematics, University of Strathclyde, UK ([james.dalby@strath.ac.uk](mailto:james.dalby@strath.ac.uk), [apala.majumdar@strath.ac.uk](mailto:apala.majumdar@strath.ac.uk), [yucen.han@strath.ac.uk](mailto:yucen.han@strath.ac.uk)).

<sup>‡</sup>Department of Mathematics and Statistics, Mount Holyoke College, Massachusetts, USA ([lmrad@mtholyoke.edu](mailto:lmrad@mtholyoke.edu)).

39 is parameterised by an angle,  $\theta$ , which describes the in-plane alignment of the nematic  
 40 molecules. In a fully 3D framework, the LdG  $\mathbf{Q}$ -tensor has five degrees of freedom  
 41 and there are exact connections between the reduced LdG and the 3D LdG descrip-  
 42 tions, as discussed in the next section. We consider steady unidirectional flows, which,  
 43 within the Beris-Edwards framework, are captured by a system of coupled differential  
 44 equations for  $s$ ,  $\theta$ , and the fluid velocity  $\mathbf{u}$ . There are three dimensionless parameters,  
 45 two of which are related to the nematic fluidity (if these parameters are important to  
 46 mention, we should say what they are. Otherwise just focus on  $L^*$  - which I think  
 47 we should do), and the third dimensionless parameter,  $L^*$ , is inversely proportional  
 48 to  $L^2$  and plays a key role in the stability of singular structures.

49 Our work is largely devoted to *Order Reconstruction* (OR) solutions (defined  
 50 precisely in section 3). OR solutions are nematic profiles with distinct director poly-  
 51 domains, separated by singular lines or singular surfaces, referred to as domain walls.  
 52 The domain walls are ('show as', not 'are'? there might be confusion between the  
 53 horizontal and vertical planes here) simply disordered regions in the plane, and would  
 54 appear as singularities in 2D optical studies but in 3D, they describe a continuous  
 55 yet rapid rotation between distinct 3D NLC configurations in the two (adjacent?)  
 56 polydomains, as in the seminal paper [34]. OR solutions are relevant for modelling  
 57 chevron or zigzag patterns observed in pressure-driven flows [1, 10], as well as in active  
 58 nematics where aligned fibers can be controlled to display a laminar flow [23]. OR  
 59 solutions have been studied in purely nematic systems, for example in [26], [9] and  
 60 [8]. However, they are not limited to purely nematic systems: for instance, OR solu-  
 61 tions exist in ferronematic systems comprising magnetic nanoparticles in NLC media  
 62 [12]. Generalized OR solutions or OR-type solutions/instabilities (defined in section  
 63 4) are also observed in smectics and cholesterics. For example, when a cell filled with  
 64 a smectic-A liquid crystal is cooled to the smectic-C phase, a chevron texture is ob-  
 65 served and has been the impetus of considerable experimental and theoretical interest  
 66 [33, 32].

67 We thus speculate that OR solutions are a universal property of partially ordered  
 68 systems, especially small systems with conflicting boundary conditions. For systems  
 69 with constant velocity and constant pressure, we prove that OR solutions only exist  
 70 for mutually orthogonal boundary conditions imposed on  $\theta$ . This is known, but we  
 71 rediscover this fact using new arguments. For all other choices of Dirichlet bound-  
 72 ary conditions for  $\theta$ , we show that OR solutions do not exist and using geometric  
 73 and comparison principles, we prove the existence of a unique, symmetric and non-  
 74 singular  $(s, \theta)$ -profile in these cases. For general flows with non-constant velocity and  
 75 pressure, in section 4, we work with large domains ( $L^* \rightarrow 0$ ) and compute asymptotic  
 76 approximations for OR-type solutions, that exhibit a singular line or domain wall in  
 77 the channel centre, for both passive and active scenarios. For OR-type solutions, the  
 78 director is not constant away from the isotropic line, as in the case of OR solutions.  
 79 Our asymptotic methods are adapted from [7], where the authors investigate a chevron  
 80 texture characterised specifically by a  $\pm\pi/4$  jump in  $\theta$ , using an Ericksen model for  
 81 uniaxial NLCs. These asymptotic methods, now placed within the Beris-Edwards  
 82 framework, allow us to explicitly construct solutions characterised by a domain wall  
 83 as described above, with a planar jump discontinuity in  $\theta$ , which we refer to as an  
 84 OR-type solution. We also construct OR-type solutions for active nematodynamics,  
 85 by working in the reduced Beris-Edwards framework with additional non-equilibrium  
 86 active stresses [18], thus illustrating the universality of OR-type solutions.

87 We validate our asymptotics for passive and active nematodynamics (with non-  
 88 constant pressure and flow), with extensive numerical experiments, for large and small

89 values of  $L^*$ . In both settings, we find OR-type solutions for all values of  $L^*$ , with  
 90 mutually orthogonal Dirichlet conditions for  $\theta$  on the channel walls. OR-type solutions  
 91 are stable for large  $L^*$ , and unstable for small  $L^*$ . In fact, we observe multiple  
 92 unstable OR-type solutions for small values of  $L^*$ . Our asymptotic expansions serve  
 93 as excellent initial conditions for numerically computing different branches of OR-  
 94 type solutions, characterised by different jumps in  $\theta$ , and the numerics agree well  
 95 with the asymptotics. We speculate that unstable OR-type solutions can potentially  
 96 be stabilised by external controls and thus, play a role in switching and dynamical  
 97 phenomena.

98 The paper is organised as follows. In section 2, we describe the Beris-Edwards  
 99 model, our channel geometry and the imposed boundary conditions. In section 3,  
 100 we study flows with constant velocity and pressure, and identify conditions which  
 101 allow and disallow OR solutions, in terms of the boundary conditions. In section  
 102 4, we compute asymptotic expansions for OR-type solutions with passive and active  
 103 nematic flows for small  $L^*$  or large channel widths, providing explicit limiting profiles  
 104 in these cases. We then supplement our analysis with detailed numerical experiments,  
 105 followed by some brief conclusions and future perspectives in section 5.

106 **2. Theory.** We consider NLCs sandwiched inside a three-dimensional (3D) chan-  
 107 nel,  $\tilde{\Omega} = \{(x, y, z) \in \mathbb{R}^3 : -D \leq x \leq D, -L \leq y \leq L, 0 \leq z \leq H\}$  where  $L, D$ , and  $H$   
 108 are the (half) width, length and height of the channel, respectively. We assume that  
 109  $D \gg L$  and  $H \ll L$ . We further assume planar surface anchoring conditions on the  
 110 top and bottom channel surfaces at  $z = 0$  and  $z = H$ , which effectively means that  
 111 the NLC molecules lie parallel to the  $xy$ -plane on these surfaces without a specified  
 112 direction, and Dirichlet or fixed boundary conditions on the lateral surfaces. Such  
 113 boundary conditions are used in experiments, see for example the planar bistable ne-  
 114 matic device in [36] and the experiments on fd-viruses in [27]. In the LdG framework,  
 115 the  $\mathbf{Q}$ -tensor order parameter is a symmetric, traceless  $3 \times 3$  matrix, with five degrees  
 116 of freedom. The physically relevant NLC configurations are modelled by minimizers of  
 117 an appropriately defined LdG free energy. In the  $H \rightarrow 0$  limit and applying Theorem  
 118 5.1 in [22] (also see Theorem 2.1 in [37]), one can show that the physically relevant  
 119 configurations are invariant in the  $z$ -direction and correspond to LdG  $\mathbf{Q}$ -tensors with  
 120 a fixed eigenvector in the  $\hat{z}$ -direction, with an associated constant eigenvalue. This  
 121 reduces the degrees of freedom from five to simply two degrees of freedom, as cap-  
 122 tured by the reduced LdG  $\mathbf{Q}$ -tensor in (2.1) below. In fact, under these assumptions,  
 123 the full LdG  $\mathbf{Q}$ -tensor is the sum of the reduced LdG  $\mathbf{Q}$ -tensor and a constant  $3 \times 3$   
 124 matrix, and it can be reconstructed from the reduced  $\mathbf{Q}$ -tensor as needed. See the  
 125 supplementary material for an explicit example connecting the reduced and full LdG  
 126  $\mathbf{Q}$ -tensors. Furthermore, since  $D \gg L$ , we assume that the system is invariant in the  
 127  $x$ -direction and this reduces our computational domain to a 1D channel,  $y \in [-L, L]$ .  
 128

129 There are two macroscopic variables in our reduced framework: the fluid velocity  
 130  $\mathbf{u}$ , and a reduced LdG  $\mathbf{Q}$ -tensor order parameter that measures the NLC orientational  
 131 ordering in the  $xy$ -plane. More precisely, the reduced  $\mathbf{Q}$ -tensor is a symmetric traceless  
 132  $2 \times 2$  matrix i.e.,  $\mathbf{Q} \in S_2 := \{\mathbf{Q} \in \mathbb{M}^{2 \times 2} : Q_{ij} = Q_{ji}, Q_{ii} = 0\}$ , which can be written  
 133 as:

$$134 \quad (2.1) \quad \mathbf{Q} = s \left( \mathbf{n} \otimes \mathbf{n} - \frac{\mathbf{I}}{2} \right).$$

135 Here,  $s$  is a scalar order parameter,  $\mathbf{n}$  is the nematic director (a unit vector describing

136 the average direction of orientational ordering in the  $xy$ -plane), and  $\mathbf{I}$  is the  $2 \times 2$   
 137 identity matrix. Moreover,  $s$  can be interpreted as a measure of the degree of order  
 138 about  $\mathbf{n}$ , so that the nodal sets of  $s$  (i.e., where  $s = 0$ ) define nematic defects in the  
 139  $xy$ -plane. As a consequence of (2.1), the two independent components of  $\mathbf{Q}$  are given  
 140 by

$$141 \quad (2.2) \quad Q_{11} = \frac{s}{2} \cos 2\theta, \quad Q_{12} = \frac{s}{2} \sin 2\theta,$$

142 when  $\mathbf{n} = (\cos \theta, \sin \theta)$ , and  $\theta$  is the angle between  $\mathbf{n}$  and the  $x$ -axis. Conversely,  
 143 applying basic trigonometric identities, we have the following relationships,

$$144 \quad (2.3) \quad s = 2\sqrt{Q_{11}^2 + Q_{12}^2} \quad \text{and} \quad \theta = \frac{1}{2} \tan^{-1} \left( \frac{Q_{12}}{Q_{11}} \right).$$

145 We work within the Beris-Edwards framework for nematodynamics [4]. There  
 146 are three governing equations: an incompressibility constraint for  $\mathbf{u}$ , an evolution  
 147 equation for  $\mathbf{u}$  (essentially the Navier–Stokes equation with an additional stress due  
 148 to the nematic ordering,  $\sigma$ ), and an evolution equation for  $\mathbf{Q}$  which has an additional  
 149 stress induced by the fluid vorticity [31]. These equations are given below,

$$150 \quad \nabla \cdot \mathbf{u} = 0, \quad \rho \frac{D\mathbf{u}}{Dt} = -\nabla p + \nabla \cdot (\mu(\nabla \mathbf{u} + (\nabla \mathbf{u})^T) + \sigma),$$

$$151 \quad \frac{D\mathbf{Q}}{Dt} = \zeta \mathbf{Q} - \mathbf{Q} \zeta + \frac{1}{\gamma} \mathbf{H}.$$

152 Here  $\rho$  and  $\mu$  are the fluid density and viscosity respectively,  $p$  is the hydrodynamic  
 153 pressure,  $\zeta$  is the anti-symmetric part of the velocity gradient tensor and  $\gamma$  is the  
 154 rotational diffusion constant. The nematic stress is defined to be

$$155 \quad \sigma = \mathbf{Q}\mathbf{H} - \mathbf{H}\mathbf{Q} \quad \text{and} \quad \mathbf{H} = \kappa \nabla^2 \mathbf{Q} - A\mathbf{Q} - C|\mathbf{Q}|^2 \mathbf{Q},$$

156 where  $\mathbf{H}$  is the molecular field related to the LdG free energy,  $\kappa$  is the nematic elasticity  
 157 constant,  $A < 0$  is a temperature dependent constant,  $C > 0$  is a material dependent  
 158 constant, and  $|\mathbf{Q}| = \sqrt{\text{Tr}(\mathbf{Q}^T \mathbf{Q})}$ , is the Frobenius norm. Finally, we assume that all  
 159 quantities depend on  $y$  alone and work with a unidirectional channel flow, so that  
 160  $\mathbf{u} = (u(y), 0)$ . The incompressibility constraint is automatically satisfied. To render  
 161 the equations nondimensional, we use the following scalings, as in [31],

$$162 \quad y = L\tilde{y}, \quad t = \frac{\gamma L^2}{\kappa} \tilde{t}, \quad u = \frac{\kappa}{\gamma L} \tilde{u}, \quad Q_{11} = \sqrt{\frac{-2A}{C}} \tilde{Q}_{11}, \quad Q_{12} = \sqrt{\frac{-2A}{C}} \tilde{Q}_{12}, \quad p_x = \frac{\mu\kappa}{\gamma L^3} \tilde{p}_x,$$

163 and then drop the tilde for simplicity. Our rescaled domain is  $\Omega = [-1, 1]$  and the  
 164 evolution equations become

$$165 \quad (2.4a) \quad \frac{\partial Q_{11}}{\partial t} = u_y Q_{12} + Q_{11,yy} + \frac{1}{L^*} Q_{11} (1 - 4(Q_{11}^2 + Q_{12}^2)),$$

$$166 \quad (2.4b) \quad \frac{\partial Q_{12}}{\partial t} = -u_y Q_{11} + Q_{12,yy} + \frac{1}{L^*} Q_{12} (1 - 4(Q_{11}^2 + Q_{12}^2)),$$

$$167 \quad (2.4c) \quad L_1 \frac{\partial u}{\partial t} = -p_x + u_{yy} + 2L_2 (Q_{11} Q_{12,yy} - Q_{12} Q_{11,yy})_y,$$

169 where  $L_1 = \frac{\rho\kappa}{\mu\gamma}$ ,  $L^* = \frac{-\kappa}{AL^2}$ , and  $L_2 = \frac{-2A\gamma}{C\mu} = \frac{-2AEr^*}{CEr}$  are dimensionless parameters.  
 170 Here,  $Er = u_0 L \mu / \kappa$  is the Ericksen number and  $Er^* = u_0 L \gamma / \kappa$  ( $u_0$  is the character-  
 171 istic length scale of the fluid velocity) is analogous to the Ericksen number in terms

172 of the rotational diffusion constant  $\gamma$ , rather than viscosity  $\mu$ . We interpret  $L^*$  as a  
 173 measure of the domain size i.e. it is the square of the ratio of two length scales: the  
 174 nematic correlation length,  $\xi = \sqrt{-\kappa/A}$  for  $A < 0$  and the domain size  $L$ , so that the  
 175  $L^* \rightarrow 0$  limit is relevant for large channels or macroscopic domains. The parameter,  
 176  $L_2$  is the product of the ratio of material and temperature-dependent constants and  
 177 the ratio of rotational to momentum diffusion [31]. In what follows, we fix  $L_1 = 1$ , and  
 178 as such do not comment on its physical significance. The static governing equations  
 179 for  $(s, \theta)$ , can be obtained from (2.4) using (2.2):

$$180 \quad (2.5a) \quad s_{yy} = 4s\theta_y^2 + \frac{1}{L^*}s(s^2 - 1),$$

$$181 \quad (2.5b) \quad s\theta_{yy} = \frac{1}{2}s u_y - 2s_y\theta_y,$$

$$183 \quad (2.5c) \quad u_{yy} = p_x - L_2(s^2\theta_y)_{yy}.$$

184 The formulation in terms of  $(s, \theta)$  gives informative insight into the solution profiles  
 185 and avoids some of the degeneracy conditions coded in the  $\mathbf{Q}$ -formulation.

186 We work with Dirichlet conditions for  $(s, \theta)$  as given below:

$$187 \quad (2.6a) \quad s(-1) = s(1) = 1,$$

$$188 \quad (2.6b) \quad \theta(-1) = -\omega\pi, \quad \theta(1) = \omega\pi,$$

190 where  $\omega \in [-\frac{1}{2}, \frac{1}{2}]$ , is the winding number. This translates to the following boundary  
 191 conditions for  $\mathbf{Q}$ :

$$192 \quad (2.7) \quad Q_{11}(\pm 1) = \frac{1}{2} \cos(2\omega\pi), \quad Q_{12}(-1) = -\frac{1}{2} \sin(2\omega\pi), \quad Q_{12}(1) = \frac{1}{2} \sin(2\omega\pi).$$

193 The boundary conditions in (2.6a) imply that the nematic molecules are perfectly  
 194 ordered on the bounding plates. We consider asymmetric Dirichlet boundary condi-  
 195 tions in (2.6b) for the angle  $\theta$ . A potential issue follows from (2.3): the range of  $\theta$  is  
 196  $(-\frac{\pi}{4}, \frac{\pi}{4})$ , but our boundary conditions extend to  $\pm\frac{\pi}{2}$ . However, we circumvent this  
 197 issue by using the function  $\text{atan2}(y, x) \in (-\pi, \pi]$ , which returns the angle between  
 the line connecting the point  $(x, y)$  to the origin and the positive  $x$  axis. For the flow

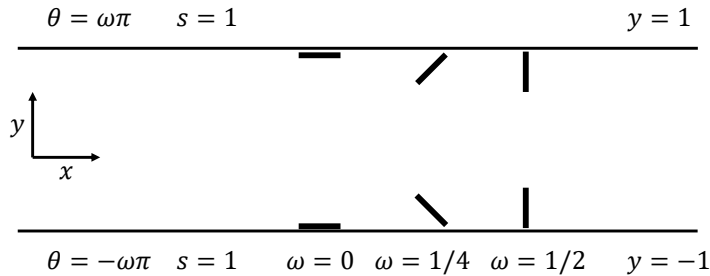


FIG. 1. Boundary conditions for  $s$  and  $\theta$ , and some example boundary conditions on the director.

198 field, we consider the typical no-slip boundary conditions, namely  
 199

$$200 \quad (2.8) \quad u(-1) = u(1) = 0,$$

202 and assume that the pressure  $p$  is uniform in the  $y$ -direction, depending on  $x$  only.

203 **3. Passive flows with constant velocity and pressure.** In this section, we  
 204 study nematic flows with constant velocity and pressure without additional activity.  
 205 This framework, though somewhat artificial, allows for OR solutions, although OR-  
 206 type solutions exist in more generic situations with non-constant flows. We work with  
 207 both the  $\mathbf{Q}$ - and  $(s, \theta)$ -frameworks in this section.

208 In our one-dimensional framework, OR solutions correspond to a partition of the  
 209 domain  $\Omega = [-1, 1]$  into sub-domains,  $\Omega = \sum_{j=1}^n \Omega_j$ , where each  $\Omega_j$  is a *polydomain*.  
 210 These polydomains have constant  $\theta$  (recall that  $\theta$  is the orientation of the planar di-  
 211 rector,  $\mathbf{n}$ ), separated by domain walls (with  $s = 0$ ) to account for **planar** jumps in  $\theta$   
 212 across polydomain boundaries. OR-type solutions are simply interpreted as solutions  
 213 of (2.4) that have a non-empty nodal set for  $s$  or exhibit domain walls, without the  
 214 constraint of constant  $\theta$  in each polydomain. In the reduced  $\mathbf{Q}$ -framework, OR so-  
 215 lutions have distinct but less obvious signatures, the domain walls correspond to the  
 216 nodal set of the reduced  $\mathbf{Q}$ -tensor. **In a 3D LdG description, the corresponding ne-**  
 217 **matic director rapidly rotates between two distinct director profiles across the domain**  
 218 **wall, and the rotation is mediated by maximal biaxiality; see supplementary mate-**  
 219 **rial.** We show, below, that OR-solutions are only compatible with specific boundary  
 220 conditions in the  $\mathbf{Q}$ -framework.

221 In the  $(s, \theta)$ -framework, OR solutions are characterised by sub-intervals with con-  
 222 stant  $\theta$ . From (2.5b), constant  $\theta$  implies constant fluid velocity  $u$  and from (2.5c),  
 223 constant pressure,  $p$ . Therefore, we assume constant velocity and pressure to start  
 224 with. In what follows,  $\prime$  denotes differentiation with respect to  $y$ .

225 In this scenario the static version of (2.4a)-(2.4b) is

$$226 \quad (3.1a) \quad Q''_{11} = \frac{1}{L^*} Q_{11} (4(Q_{11}^2 + Q_{12}^2) - 1),$$

$$227 \quad (3.1b) \quad Q''_{12} = \frac{1}{L^*} Q_{12} (4(Q_{11}^2 + Q_{12}^2) - 1).$$

229 From these equations it follows that (2.4c) is satisfied. The equations (3.1a)-(3.1b)  
 230 are the Euler-Lagrange equations associated with the energy

$$231 \quad (3.2) \quad F_{LG}[Q_{11}, Q_{12}] = \int_{\Omega} \left( (Q'_{11})^2 + (Q'_{12})^2 \right) + \frac{1}{L^*} (Q_{11}^2 + Q_{12}^2) (2(Q_{11}^2 + Q_{12}^2) - 1) \, dy.$$

233 The admissible  $\mathbf{Q}$ -tensors belong to the Sobolev space,  $W^{1,2}([-1, 1]; S_2)$ , where  $S_2$  is  
 234 the space of symmetric and traceless  $2 \times 2$  matrices, subject to appropriately defined  
 235 boundary conditions (see (2.7)). The stable and physically observable configurations  
 236 correspond to local or global minimizers of (3.2), in the prescribed admissible space.

237 In the static case, with constant  $u$  and  $p$ , the corresponding equations for  $(s, \theta)$   
 238 can be deduced from (2.5a), (2.5b) :

$$239 \quad (3.3a) \quad s'' = 4s(\theta')^2 + \frac{1}{L^*} s(s^2 - 1),$$

$$240 \quad (3.3b) \quad (s^2 \theta')' = 0, \implies s^2 \theta' = B,$$

242 whilst (2.5c) is automatically satisfied. In the above,  $B$  is a fixed constant of integra-  
 243 tion; in fact

$$244 \quad (3.4) \quad B = \theta'(-1) = \theta'(1).$$

245 When  $\omega \geq 0$  and recalling the boundary conditions for  $\theta$ , there exists a point  $y_0$   
 246 such that  $\theta'(y_0) \geq 0$ , hence  $B \geq 0$ , and  $\theta' \geq 0$  for all  $y \in [-1, 1]$ . Thus, we have

$$247 \quad (3.5) \quad -\omega\pi \leq \theta \leq \omega\pi, \quad \forall y \in [-1, 1] \text{ and } \forall \omega \in \left[0, \frac{1}{2}\right].$$

248 Similar comments apply when  $\omega \leq 0$ , for which  $B \leq 0$ , and  $\theta' \leq 0$  for all  $y \in [-1, 1]$ .  
 249 If  $B = 0$ , we either have  $s = 0$  or  $\theta = \text{constant}$  almost everywhere, compatible with  
 250 the definition of an OR solution (unless  $\omega = 0$ , and  $(s, \theta) = (1, 0)$ , which is not an  
 251 OR solution). Conversely, an OR solution, by definition, has  $B = 0$  since polydomain  
 252 structures correspond to piecewise constant  $\theta$ -profiles. In other words, if  $\omega \neq 0$ , OR  
 253 solutions exist if and only if  $B = 0$ . If  $B \neq 0$ , then OR solutions are necessarily  
 254 disallowed because a non-zero value of  $B$  implies that  $s \neq 0$  on  $\Omega$ . The following  
 255 results show that the choice of  $B$  is in turn dictated by  $\omega$ , or the Dirichlet boundary  
 256 conditions, and this sheds beautiful insight into how the boundary datum manifests  
 257 in the multiplicity and regularity of solutions. In what follows, we let  $\epsilon := \frac{1}{L^\alpha}$ , so that  
 258  $\epsilon \propto L^2$  where  $L$  is the physical channel width.

259 Note that (3.3a) and (3.3b) are the Euler-Lagrange equations of the following  
 260 energy,

$$261 \quad (3.6) \quad F_{LG}[s, \theta] = \int_{\Omega} \left( \frac{(s')^2}{4} + s^2(\theta')^2 \right) + \frac{\epsilon s^2}{4} \left( \frac{s^2}{2} - 1 \right) dy,$$

263 but we only consider  $(s, \theta) \in W^{1,2}(\Omega; \mathbb{R})$  and focus on smooth, classical solutions of  
 264 (3.3a) and (3.3b), subject to the boundary conditions in (2.6a)-(2.6b), and not OR  
 265 solutions. We first prove that OR solutions only exist for the special values,  $\omega = \pm \frac{1}{4}$ ,  
 266 in the **Q**-framework. If  $\omega = \pm \frac{1}{4}$ , then  $B$  can be either zero or non-zero for differ-  
 267 ent solution branches, especially for small values of  $\epsilon$  that admit multiple solution  
 268 branches. Once the correspondence between  $\omega$ ,  $B$  and OR solutions is established  
 269 **in the Q-framework**, we proceed to prove several qualitative properties of the cor-  
 270 responding  $(s, \theta)$ -profiles which are of independent interest, followed by asymptotics  
 271 and numerical experiments (also see supplementary material).

272 **THEOREM 3.1.** *For all  $\epsilon \geq 0$ , there exists a minimizer of the energy (3.2), in the*  
 273 *admissible space*

$$275 \quad (3.7) \quad \mathcal{A} = \left\{ \mathbf{Q} \in W^{1,2}([-1, 1]; S_2); Q_{11}(\pm 1) = \frac{\cos(2\omega\pi)}{2}, \right. \\ \left. Q_{12}(-1) = -\frac{\sin 2\omega\pi}{2}, Q_{12}(1) = \frac{\sin 2\omega\pi}{2} \right\}.$$

278 *Moreover, the system (3.1) admits an analytic solution for all  $\epsilon \geq 0$ , in  $\mathcal{A}$ . OR*  
 279 *solutions only exist for  $\omega = \pm \frac{1}{4}$  in (2.7).*

280 *Proof.* The existence of an energy minimizer for (3.2) in  $\mathcal{A}$ , is immediate from the  
 281 direct methods in the calculus of variations, for all  $\epsilon$  and  $\omega$ , and the minimizer is a  
 282 classical solution of the associated Euler-Lagrange equations (3.1), for all  $\epsilon$  and  $\omega$ . In  
 283 fact, using standard arguments in elliptic regularity, one can show that all solutions  
 284 of the system (3.1) are analytic [5].

285 The key observation is

$$286 \quad (Q'_{12}Q_{11} - Q'_{11}Q_{12})' = Q''_{12}Q_{11} + Q'_{12}Q'_{11} - Q'_{12}Q'_{11} - Q_{12}Q''_{11} = 0,$$

287 and hence,  $Q'_{12}Q_{11} - Q'_{11}Q_{12}$  is a constant. In fact, using (2.3), we see that

$$288 \quad (s^2\theta')' = 2(Q'_{12}Q_{11} - Q'_{11}Q_{12}) = 0 \implies s^2\theta' = 2(Q'_{12}Q_{11} - Q'_{11}Q_{12}) = B,$$

289 where  $B$  is as in (2.5b). Now let  $B = 0$  (so that OR solutions are possible), then

$$290 \quad (3.8) \quad Q'_{12}Q_{11} = Q'_{11}Q_{12} \text{ for all } y \in [-1, 1].$$

291 There are two obvious solutions of (3.8) i.e.  $Q_{11} \equiv 0$  (i.e.,  $\omega = \pm\frac{1}{4}$ ), or  $Q_{12} \equiv 0$  (i.e.,  
292  $\omega = 0, \pm\frac{1}{2}$ ), everywhere on  $\Omega$ . For the case  $Q_{12} \equiv 0$  and  $\omega = \pm\frac{1}{2}$ , the Euler-Lagrange  
293 equations for  $\mathbf{Q}$  reduce to

$$294 \quad (3.9) \quad \begin{cases} Q''_{11} = \epsilon Q_{11}(4Q_{11}^2 - 1), \\ Q_{11}(-1) = -\frac{1}{2}, Q_{11}(1) = -\frac{1}{2}. \end{cases}$$

295 This is essentially the ODE considered in equation (20) of [26]. Applying the argu-  
296 ments in Lemma 5.4 of [26], the solution  $Q_{11}$  of (3.9) must satisfy  $Q'_{11}(-1) = 0$ , or  
297  $Q'_{11}$  is always positive. However, the latter is not possible since we have symmet-  
298 ric boundary conditions. Hence, when  $\omega = \pm\frac{1}{2}$ , the unique solution to (3.9) is the  
299 constant solution  $(Q_{11}, Q_{12}) = (-\frac{1}{2}, 0)$ . This corresponds to  $s = 1$  everywhere in  $\Omega$ ,  
300 which is not an OR solution. The same arguments apply to the case  $Q_{12} \equiv 0$  and  
301  $\omega = 0$ . In this case the boundary conditions are  $Q_{11}(\pm 1) = \frac{1}{2}$ , and the corresponding  
302  $(s, \theta)$  solution is simply,  $(s, \theta) = (1, 0)$ , which is again not an OR solution.

303 When  $Q_{11} \equiv 0$  ( $\omega = \pm\frac{1}{4}$ ), the  $\mathbf{Q}$  system becomes

$$304 \quad (3.10) \quad \begin{cases} Q''_{12} = \epsilon Q_{12}(4Q_{12}^2 - 1), \\ Q_{12}(-1) = -\frac{1}{2}, Q_{12}(1) = \frac{1}{2}. \end{cases}$$

305 Applying the arguments in Lemma 5.4 of [26], we see (3.10) has a unique solution  
306 which is odd and increasing, with a single zero at  $y = 0$  - the centre of the channel.  
307 This is an OR solution, since  $Q_{11} = 0$  implies that  $\theta$  is constant on either side of  
308  $y = 0$ .

309 It remains to show that there are no solutions  $(Q_{11}, Q_{12})$  of (3.1), which satisfy  
310 (3.8), other than the possibilities considered above. To this end, we assume that  
311 we have non-trivial solutions,  $Q_{11}$  and  $Q_{12}$  such that (3.8) holds. We recall that all  
312 solution pairs,  $(Q_{11}, Q_{12})$  of (3.1) are analytic and hence, can only have zeroes at  
313 isolated interior points of  $\Omega = [-1, 1]$ . This means that there exists a finite number  
314 of intervals  $(-1, y_1), \dots, (y_n, 1)$ , such that  $Q_{11} \neq 0$  and  $Q_{12} \neq 0$  in the interior of  
315 these intervals, whilst either  $Q_{11}(y_i)$ ,  $Q_{12}(y_i)$ , or both, equal zero at each intervals  
316 end-points. We then have that

$$317 \quad \frac{Q'_{12}}{Q_{12}} = \frac{Q'_{11}}{Q_{11}} \implies |Q_{11}| = c_i |Q_{12}| \text{ for } y \in (y_{i-1}, y_i)$$

318 for constants  $c_i > 0$  and  $i = 1, \dots, n$ . Therefore, there exists an interval,  $(y_{i-1}, y_i)$ ,  
319 for which  $Q_{11}$  and  $Q_{12}$  have the same, or opposite signs. Assume without loss of  
320 generality (W.L.O.G.)  $Q_{11}$  and  $Q_{12}$  have the same sign, then the analytic function

$$321 \quad f(y) := Q_{11}(y) - c_i Q_{12}(y) = 0, \text{ for } y \in (y_{i-1}, y_i).$$

322 Therefore,  $f(y) = 0$  for all  $y \in [-1, 1]$ . Evaluating at  $y = \pm 1$ , we have

$$323 \quad \cos(2\omega\pi) = -\sin(2\omega\pi)c_i \text{ and } \cos(2\omega\pi) = \sin(2\omega\pi)c_i,$$

324 and this is only possible if  $\cos(2\omega\pi) = 0$  and  $\sin(2\omega\pi)c_i = 0$ , which implies  $\omega = \pm\frac{1}{4}$   
 325 and  $c_i = 0$ . Hence, there are only three possibilities for  $\omega = 0, \pm\frac{1}{4}, \pm\frac{1}{2}$  that are  
 326 consistent with (3.8), of which OR solutions are only compatible with  $\omega = \pm\frac{1}{4}$ .  $\square$

327 In what follows, we consider the solution profiles,  $(s, \theta)$  of (3.3a) and (3.3b), from  
 328 which we can construct a solution of the system (3.1), using the definitions (2.2). The  
 329 first proposition below is adapted from [29], although some additional work is needed  
 330 to deal with the positivity of  $s$ ; see the supplementary material.

331 **THEOREM 3.2. (Maximum Principle)** *Let  $s$  and  $\theta$  be solutions of (3.3a) and*  
 332 *(3.3b), where  $s$  is at least  $C^2$  and  $\theta$  is at least  $C^1$ , then*

$$333 \quad (3.11) \quad 0 < s \leq 1 \quad \forall y \in [-1, 1].$$

334 For the next batch of results, we omit the case  $B = 0$  and focus on the  $(s, \theta)$ -  
 335 profiles of non OR-solutions, which are necessarily smooth. We exploit this fact  
 336 to prove that there exists a unique solution pair,  $(s, \theta)$  of (3.3), such that  $s$  has a  
 337 symmetric even profile about  $y = 0$ , for every  $B \neq 0$ .

338 **THEOREM 3.3.** *Any non-constant and non-OR solution,  $s$ , of the Euler-Lagrange*  
 339 *equations (3.3), has a single critical point which is necessarily a non-trivial global*  
 340 *minimum at some  $y^* \in (-1, 1)$ .*

341 *Proof.* For clarity, we denote a specific solution of (3.3a) and (3.3b), by  $(s_{sol}, \theta_{sol})$   
 342 in this proof. Recall that for non-OR solutions, we necessarily have  $B = \theta'(\pm 1) \neq 0$   
 343 and  $s \neq 0$  anywhere. Using the definition of  $B$  in (3.3), we have

$$344 \quad (3.12) \quad s'' = \frac{4B^2}{s^3} + \epsilon(s^3 - s).$$

345 The right hand side of (3.12) is well-defined and continuous for  $s \in (0, 1]$ , and as such,  
 346 a solution,  $s_{sol}$ , will be  $C^2$ . In fact, the right hand side of (3.12) is smooth, hence  
 347 any solution,  $s_{sol}$ , will be smooth. The boundary conditions,  $s(\pm 1) = 1$ , imply that  
 348 a non-trivial solution has  $s'_{sol}(y^*) = 0$  for some  $y^* \in [-1, 1]$ , where  $s'$  is defined as,

$$349 \quad (3.13) \quad s' = \pm \sqrt{\left(-4B^2s^{-2} + \epsilon\left(\frac{s^4}{2} - s^2\right) + J\right)}.$$

350 Here,  $A$  is a constant of integration and  $J = 4B^2 + \frac{\epsilon}{2} + s'(\pm 1)^2$ , hence, we must have

$$351 \quad (3.14) \quad J \geq 4B^2 + \frac{\epsilon}{2}.$$

352 Since  $s'$  is defined in terms of  $s$  and not  $y$ , solutions of  $s' = 0$  give us the extrema  
 353 of a solution  $s_{sol}$  (i.e., maxima or minima), rather than the location of the critical  
 354 points on the  $y$ -axis. The condition  $s' = 0$  is equivalent to

$$355 \quad (3.15) \quad J = 4B^2s^{-2} - \epsilon\left(\frac{s^4}{2} - s^2\right).$$

356 Clearly if  $\epsilon = 0$ , we can only have one extremum, namely  $s = \sqrt{\frac{4B^2}{J}}$ , which in view  
 357 of the boundary conditions and maximum principle, must be a minimum. For  $\epsilon > 0$ ,  
 358 solving (3.15) is equivalent to computing the roots of  $f(s) = 0$  where

$$359 \quad (3.16) \quad f(s) := s^6 - 2s^4 + \frac{2J}{\epsilon}s^2 - \frac{8B^2}{\epsilon}.$$

360 Firstly, note that  $f$  has a root for  $s \in (0, 1]$ , since  $f(0) = \frac{-8B^2}{\epsilon} < 0$  and  $f(1) =$   
 361  $-1 + \frac{2J}{\epsilon} - \frac{8B^2}{\epsilon} \geq 0$ , by (3.14). Differentiating (3.16), we obtain

$$362 \quad \frac{df}{ds}(s) = 6s^5 - 8s^3 + \frac{4J}{\epsilon}s,$$

363 and the critical points of  $f$  are given by

$$364 \quad (3.17) \quad s = 0, \quad s_{\pm} = \sqrt{\frac{8 \pm \sqrt{64 - \frac{96J}{\epsilon}}}{12}},$$

365 provided that  $A \leq \frac{2}{3\sqrt{3}}\epsilon$ . There are now three cases to consider.

366 Case 1: If  $J > \frac{3\sqrt{3}}{2}\epsilon$ ,  $f(s)$  has one critical point at  $s = 0$ , which is a negative global  
 367 minimum. Hence,  $f$  has one root in the range,  $s \in (0, 1]$ .

368 Case 2: Let  $J = \frac{2}{3}\epsilon$ , so that the two critical points  $s_{\pm}$  coincide. The point  $s = 0$   
 369 is still a minimum of  $f(s)$  and the coefficient of  $s^6$  is positive (so  $f \rightarrow \infty$  as  $s \rightarrow \infty$ ),  
 370 so we deduce that  $s_{\pm}$  is a stationary point of inflection (this can be checked via direct  
 371 computation). So again,  $f$  has one root for  $s \in (0, 1]$ .

372 Case 3: Finally, let  $J < \frac{2}{3}\epsilon$ , so that  $s_{\pm}$  are distinct critical points of  $f$ . The point,  
 373  $s = 0$ , is still a minimum of  $f(s)$  and the coefficient of  $s^6$  is positive, so that there  
 374 are two possibilities: (a)  $s_{\pm}$  are distinct saddle points, and since  $f$  is increasing for  
 375  $s > 0$ , we see  $f$  has a single root for  $s \in (0, 1]$ , or (b)  $s_-$  is a local maximum and  $s_+$   
 376 is a local minimum of  $f(s)$ . In the latter case,  $s = 0$  is still a global minimum for  
 377  $f(s)$ , because  $f(s_+) > f(0)$ . Using this information, we can produce a sketch of  $f(s)$   
 378 (shown in Figure 2), and there are 5 cases to consider for the number of roots of  $f$ .

379 In cases (i) and (v) of Figure 2,  $f$  has only one root for  $s \in (0, 1]$ . Next, in order  
 380 for the derivative  $s'_{sol}$  to be real, the term under the square root in (3.13), has to be  
 381 non-negative. This requires that  $f(s) \geq 0$  for all  $s \in [c, 1]$ , for some  $c > 0$ . Applying  
 382 this argument to cases (ii) and (iii) in Figure 2 by omitting regions with  $f(s) < 0$ , we  
 383 deduce that  $f$  has a single non-trivial root for  $s \in (0, 1]$ .

384 For case (iv), we have two distinct roots in an interval such that  $f(s) \geq 0$ , one of  
 385 which is  $s_+$ , and the other root is labelled as  $s_1$ . Recalling that  $s_+$  is also a solution  
 386 of  $f'(s) = 0$ , we deduce that  $s_+$  is a repeated root of  $f$ . Then,  $f$  can be factorised as:

$$387 \quad f(s) = (s - s_+)^2(s + s_+)^2(s - s_1)(s + s_1)$$

$$388 \quad (3.18) \quad = s^6 - (2s_+^2 + s_1^2)s^4 + (s_+^4 + 2s_1^2s_+^2)s^2 - s_1^2s_+^4.$$

390 Comparing the coefficient of  $s^4$  and  $s^0$  in (3.16), with (3.18), we have  $s_1^2 = 2(1 - s_+^2)$   
 391 and  $s_1^2 = \frac{8B^2}{\epsilon s_+^4}$ , which implies

$$392 \quad (3.19) \quad 4B^2 + \epsilon s_+^4(s_+^2 - 1) = 0.$$

393 Comparing (3.12) with (3.19), we deduce that,  $s''(s_+) = 0$ . By the uniqueness theory  
 394 for Cauchy problems, this implies that  $s_{sol} \equiv s_+$ , which is inadmissible and this case  
 395 is excluded.

396 In cases 1, 2 and 3, we have demonstrated that  $s_{sol}$  has a unique positive critical  
 397 value, which must be the minimum value. The unique minimum value is attained at  
 398 a unique interior point (if there were two interior minima at say  $y^*$  and  $y^{**}$ , a non-  
 399 constant solution would exhibit a local maximum between the two minima, which is  
 400 excluded by a unique critical value for  $s_{sol}$ ). This completes the proof.  $\square$

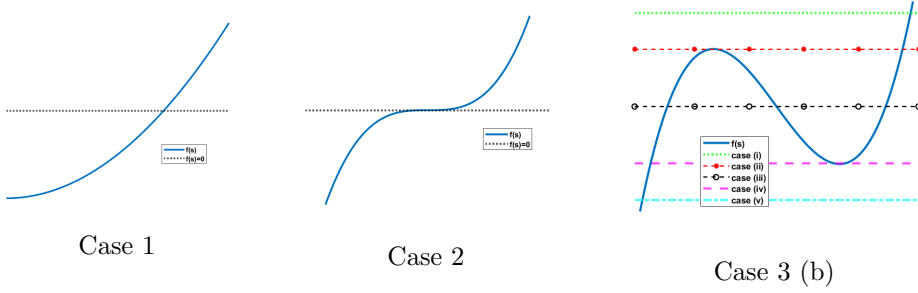


FIG. 2. The horizontal lines represent  $f(s) = 0$ .

401 THEOREM 3.4. For a given  $B = \theta'(\pm 1) \neq 0$ , the system (3.3), subject to the  
 402 boundary conditions (2.6), admits a unique solution for a fixed  $\epsilon$  and  $\omega$ . Hence, for  
 403 any value of  $\omega$  that does not permit OR solutions, the system (3.3) always has a  
 404 unique solution.

405 *Proof.* Recall, for  $\omega \neq 0$ , OR solutions exist if and only if  $B = 0$ . When  $\omega = 0$ ,  
 406 (3.3b) implies we must have  $B = 0$ , the proof of Theorem 3.2 (see supplementary  
 407 material) then shows the unique solution in  $W^{1,2}$  is  $(s, \theta) = (1, 0)$ . For  $B \neq 0$ , the  
 408 system (3.3) can be written as

$$409 \quad (3.20a) \quad s'' = \frac{4B^2}{s^3} + \epsilon s(s^2 - 1),$$

$$410 \quad (3.20b) \quad s^2 \theta' = B.$$

412 Throughout this proof we take  $B > 0$ , so that  $s \neq 0$  and hence, the right hand side  
 413 of (3.20a) is analytic. The case  $B < 0$  can be tackled in the same manner.

414 In the first step, we show that (3.20) has a unique solution for fixed  $B$ ,  $\epsilon$  and  
 415  $\omega$ . Assume for contradiction that  $(s_1, \theta_1)$  and  $(s_2, \theta_2)$  are distinct solutions pairs of  
 416 (3.20), which satisfy (2.6). As such, they must have distinct derivatives at  $y = -1$   
 417 (otherwise they would satisfy the same Cauchy problem). Suppose W.L.O.G.

$$418 \quad (3.21) \quad s_1'(-1) < s_2'(-1) \leq 0.$$

419 Since  $s_1(1) = s_2(1) = 1$ , there exists  $y_0 = \min\{y > -1 : s_1(y) = s_2(y) := s_0\}$ .  
 420 Therefore,  $s_1 < s_2$  for all  $y \in (-1, y_0)$ . Further, since  $s_1$  and  $s_2$  have one non-trivial  
 421 global minimum (Theorem 3.3), there are four possibilities for the location of  $y_0$ : (i)  
 422 Case I:  $y_0 = 1$ ; (ii) Case II:  $y_0 < \min\{\alpha, \beta\}$  where  $s_1$  attains its unique minimum at  
 423  $y = \alpha$  and  $s_2$  attains its unique minimum at  $y = \beta$ ; (iii) Case III:  $\alpha \leq y_0 \leq \beta$ , or  
 424  $\beta \leq y_0 \leq \alpha$ ; and (iv) Case IV:  $y_0 > \max\{\alpha, \beta\}$ . In case I,  $s_1 < s_2$  implies  $\theta_1' > \theta_2'$   
 425 for all  $y \in (-1, 1)$ , since both solution pairs satisfy (3.20b). Hence,  $\theta_1(y) - \theta_2(y)$   
 426 is increasing, and cannot vanish at  $y = 1$ , contradicting the boundary condition at  
 427  $y = 1$ .

428 For Case II, we have

$$429 \quad s_2'(y_0) \leq s_1'(y_0) < 0$$

430 so that

$$431 \quad (s_2'(-1))^2 - (s_2'(y_0))^2 < (s_1'(-1))^2 - (s_1'(y_0))^2.$$

432 Using (3.13), this is equivalent to

433

$$434 \quad -4B^2 - \frac{\epsilon}{2} + J_2 - \left( -\frac{4B^2}{s_0^2} + \epsilon s_0^2 \left( \frac{s_0^2}{2} - 1 \right) + J_2 \right) <$$

$$435 \quad -4B^2 - \frac{\epsilon}{2} + J_1 - \left( -\frac{4B^2}{s_0^2} + \epsilon s_0^2 \left( \frac{s_0^2}{2} - 1 \right) + J_1 \right),$$

436

437 where  $J_1$  and  $J_2$  are constants of integration associated with  $s_1$  and  $s_2$  respectively,  
 438 and may not be equal. However, the left and right hand sides are in fact equal,  
 439 yielding the desired contradiction.

440 For Cases III and IV, there must exist another point of intersection,  $y = y_1 \in$   
 441  $(\max\{\alpha, \beta\}, 1]$ , such that

$$442 \quad (s_1 - s_2)(y_1) = 0; \quad (s_1 - s_2)'(y_1) < 0$$

443 and

$$444 \quad 0 < s_1'(y_1) \leq s_2'(y_1).$$

445 In this case, we can use

$$446 \quad (s_2'(-1))^2 - (s_2'(y_1))^2 < (s_1'(-1))^2 - (s_1'(y_1))^2$$

447 to get the desired contradiction. We therefore conclude that for fixed  $B$ ,  $\epsilon$  and  $\omega$ , the  
 448 solution of (3.3) is unique.

449 Next, we show the constant  $B$  is unique for fixed  $\epsilon$  and  $\omega$ . We assume that there  
 450 exist two distinct solution pairs,  $(s_1, \theta_1)$  and  $(s_2, \theta_2)$ , which by the first part of the  
 451 proof, are the unique solutions of

$$452 \quad s_1'' = \frac{4B_1^2}{s_1^3} + \epsilon s_1(s_1^2 - 1), \quad s_2'' = \frac{4B_2^2}{s_2^3} + \epsilon s_2(s_2^2 - 1)$$

453

454 and  $s_1^2 \theta_1' = B_1$ ,  $s_2^2 \theta_2' = B_2$ , respectively, subject to (2.6), for the same value of  $\omega$ . Let  
 455  $0 < B_1 \leq B_2$ . Using a change of variable  $u_k = 1 - s_k \in [0, 1]$ , for  $k = 1, 2$  so that  
 456  $u_k(\pm 1) = 0$ , we can use the method of sub- and supersolutions to deduce that

$$457 \quad (3.22) \quad s_2 \leq s_1 \text{ for all } y \in [-1, 1].$$

458 This implies

$$459 \quad (3.23) \quad \theta_1' = \frac{B_1}{s_1^2} \leq \frac{B_2}{s_2^2} = \theta_2' \quad \forall y \in [-1, 1].$$

460 If  $\theta_1' < \theta_2'$  anywhere, then  $\theta_1(1) = \omega\pi$  does not hold, hence we must have equality  
 461 i.e.,  $\theta_1' = \theta_2'$ . It therefore follows that  $B_1 s_1^2 = B_2 s_2^2$ , but the boundary conditions  
 462 necessitate that  $B_1 = B_2 := B$  and hence,  $s_1 = s_2 := s$ . Finally, integrating  $\theta_1' =$   
 463  $B/s^2$ , it follows that  $\theta_1$  is unique and is given by

$$464 \quad (3.24) \quad \theta_1(y) = \omega\pi - \int_y^1 \frac{B}{s^2} dy, \text{ where } B = 2\omega\pi \left( \int_{-1}^1 \frac{1}{s^2} dy \right)^{-1}.$$

465 The preceding arguments show that  $\theta_1 = \theta_2$  and the proof is complete.  $\square$

466 THEOREM 3.5. For  $B = \theta'(\pm 1) \neq 0$ , the unique solution,  $(s, \theta)$  of (3.3), has the  
 467 following symmetry properties:

$$468 \quad s(y) = s(-y) \quad \theta(y) = -\theta(-y)$$

469 for all  $y \in [-1, 1]$ . Then  $s$  has a unique non-trivial minimum at  $y = 0$ .

470 *Proof.* It can be readily checked that for  $B \neq 0$ , the system of equations (3.3)  
 471 admits a solution pair,  $(s, \theta)$  such that  $s$  is even, and  $\theta$  is odd for  $y \in [-1, 1]$ , compatible  
 472 with the boundary conditions. Combining this observation with the uniqueness result  
 473 for  $B \neq 0$ , the conclusion of the theorem follows.  $\square$

474 The preceding results apply to non OR-solutions. OR solution-branches have  
 475 been studied in detail, in a one-dimensional setting, in the  $\mathbf{Q}$ -framework [26]. Using  
 476 the arguments in [26], one can prove that for  $\omega = \pm \frac{1}{4}$ , OR solutions exist for all  
 477  $\epsilon \geq 0$  and are globally stable as  $\epsilon \rightarrow 0$ , but lose stability as  $\epsilon$  increases. In particular,  
 478 non-OR solutions emerge as  $\epsilon$  increases, for  $\omega = \pm \frac{1}{4}$ , and these non-OR solutions do  
 479 not have polydomain structures. More precisely, we can explicitly compute limiting  
 480 profiles in the  $\epsilon \rightarrow 0$  and  $\epsilon \rightarrow \infty$  limits. **These calculations (which yield good insight**  
 481 **into the more complex cases of non-constant velocity and pressure for passive and**  
 482 **active nematodynamics considered next) can be found in the supplementary material**  
 483 **([16],[24],[6] are associated new references appearing in the supplementary material).**  
 484

485 **4. Passive and Active flows.** In this section, we compute asymptotic expansions  
 486 for OR-type solutions of the system (2.5), in the  $L^* \rightarrow 0$  limit ( $\epsilon \rightarrow \infty$  limit)  
 487 relevant to micron-scale channels. We consider conventional passive nematodynamics  
 488 and active nematodynamics (with additional stresses generated by internal activity),  
 489 and generic scenarios with non-constant velocity and pressure. We follow the asymp-  
 490 totic methods in [7] to construct OR-type solutions, strongly reminiscent of chevron  
 491 patterns seen in experiments [1, 10]. Recall an OR-type solution is simply a solution  
 492 of (2.5) with a non-empty nodal set for the scalar order parameter, such that  $\theta$  has a  
 493 **planar** jump discontinuity at the zeroes of  $s$ . Unlike OR solutions, OR-type solutions  
 494 need not have polydomains with constant  $\theta$ -profiles.

495 **4.1. Asymptotics for OR-type solutions in passive nematodynamics, in**  
 496 **the  $L^* \rightarrow 0$  limit.** Consider the system, (2.5), in the  $L^* \rightarrow 0$  limit. Motivated by  
 497 the results of section 3, and for simplicity, we assume  $s$  attains a single minimum at  
 498  $y = 0$ ,  $s$  is even and  $\theta$  is odd, throughout this section. The first step is to calculate  
 499 the flow gradient  $u_y$ . We multiply (2.5b) by  $s$  so that

$$500 \quad (4.1) \quad (s^2\theta_y)_y = \frac{s^2}{2}u_y.$$

501 Substituting  $(s^2\theta_y)_y$  from (4.1) into (2.5c), we obtain

$$502 \quad (4.2) \quad \left( u_y + \frac{L_2}{2}s^2u_y \right)_y = p_x.$$

503 Both sides of (4.2) equal a constant, since the left hand side is independent of  $x$ , and  
 504  $p_x$  is independent of  $y$ . Integrating (4.2), we find

$$505 \quad (4.3) \quad u_y = \frac{p_x y}{g(s)} + \frac{B_0}{g(s)},$$

506 where  $B_0$  is another constant and

$$507 \quad (4.4) \quad g(s) = 1 + \frac{L_2}{2}s^2 > 0, \quad \forall s \in \mathbb{R}.$$

508 Integrating (4.3), we have

$$509 \quad (4.5) \quad u(y) = \int_{-1}^y \frac{p_x Y}{g(s(Y))} + \frac{B_0}{g(s(Y))} dY,$$

510 since  $u(-1) = 0$  from (2.8). Using the no-slip condition,  $u(1) = 0$  and the fact  
 511 that  $\int_{-1}^1 \frac{Y}{g(s(Y))} dY = 0$ , we obtain  $B_0 = 0$  so that the flow velocity is given by  
 512  $u(y) = \int_{-1}^y \frac{p_x Y}{g(s(Y))} dY$ , and the corresponding velocity gradient is

$$513 \quad (4.6) \quad u_y(y) = \frac{p_x y}{g(s)}.$$

514 Following the method in [7], we assume

$$515 \quad (4.7a) \quad s(y) = S(y) + IS(\lambda) + \mathcal{O}(L^*),$$

$$516 \quad (4.7b) \quad \theta(y) = \Theta(y) + I\Theta(\lambda) + \mathcal{O}(L^*),$$

518 where  $S, \Theta$  represent the outer solutions away from the jump point at  $y = 0$ ,  $IS, I\Theta$   
 519 represent the inner solutions around  $y = 0$ , and  $\lambda$  is our inner variable. Substituting  
 520 these expansions into (2.5a) and (2.5b) yields

$$521 \quad (4.8a) \quad L^* S_{yy} + L^* IS_{yy} = 4L^*(S + IS)(\Theta_y + I\Theta_y)^2 + (S + IS)((S + IS)^2 - 1),$$

$$522 \quad (4.8b) \quad (S + IS)(\Theta_{yy} + I\Theta_{yy}) = \frac{1}{2}(S + IS)u_y(y) - 2(S_y + IS_y)(\Theta_y + I\Theta_y).$$

524 It is clear that (4.8a) is a singular problem in the  $L^* \rightarrow 0$  limit, and as such we rescale  
 525  $y$  and set

$$526 \quad (4.9) \quad \lambda = \frac{y}{\sqrt{L^*}},$$

527 to be our inner variable.

528 The outer solution is simply the solution of (4.8a) and (4.8b), away from  $y = 0$ ,  
 529 for  $L^* = 0$  and when internal contributions are ignored. In this case, (4.8a) reduces  
 530 to

$$531 \quad (4.10) \quad S(S^2 - 1) = 0,$$

532 which implies

$$533 \quad (4.11) \quad S(y) = 1, \quad \text{for } y \in [-1, 0) \cap (0, 1]$$

534 is the outer solution. Here we have ignored the trivial solution  $S = 0$ , and  $S = -1$ ,  
 535 as these solutions do not satisfy the boundary conditions.

536 Ignoring internal contributions, (4.8b) reduces to

$$537 \quad (4.12) \quad \Theta_{yy}(y) = \frac{1}{2}u_y(y) \quad \text{for } y \in [-1, 0) \cap (0, 1].$$

538 From the above,  $s = 1$  for  $y \in [-1, 0) \cup (0, 1]$ , therefore, integrating (4.6) and imposing  
539 the no-slip boundary conditions (2.8), we obtain

$$540 \quad (4.13) \quad u(y) = \frac{p_x}{2 + L_2}(y^2 - 1).$$

542 We take  $u(0) = -\frac{p_x}{2+L_2}$ , consistent with the above expression. Solving for  $0 < y \leq 1$ ,  
543 we integrate (4.12) to obtain

$$544 \quad \Theta_y(y) = \int_0^y \frac{u_y(Y)}{2} dY + \Theta_y(0+)$$

$$545 \quad (4.14) \quad \implies \Theta_y(y) = \frac{u(y) - u(0)}{2} + \Theta_y(0+).$$

547 Similarly, for  $-1 \leq y < 0$ , integrating (4.12) yields

$$548 \quad (4.15) \quad \Theta_y(y) = \frac{u(y) - u(0)}{2} + \Theta_y(0-).$$

550 Since  $\Theta_y(0\pm)$  is unknown, we enforce the following boundary conditions at  $y = 0$   
551 to give us an explicitly computable expression

$$552 \quad (4.16a) \quad \Theta(0+) = \omega\pi - \frac{k\pi}{2}, \quad k \in \mathbb{Z},$$

$$553 \quad (4.16b) \quad \Theta(0-) = -\omega\pi + \frac{k\pi}{2}, \quad k \in \mathbb{Z}.$$

555 We now justify this jump condition. In the case of constant flow and pressure, OR  
556 solutions jump by  $\pm 2\omega\pi$ , but OR-type solutions could have different jump conditions  
557 across the domain walls, hence the inclusion of the  $\frac{k\pi}{2}$  term. **(Other jump terms are**  
558 **also possible.)** Substituting (4.13) into (4.14), integrating, and imposing the boundary  
559 conditions, we have that

$$560 \quad (4.17) \quad \Theta(y) = \frac{p_x}{(2 + L_2)} \left( \frac{y^3}{6} - \frac{y}{6} \right) + \frac{k\pi}{2}(y - 1) + \omega\pi \quad \text{for } y \in (0, 1].$$

562 Analogously, (4.15) yields

$$563 \quad (4.18) \quad \Theta(y) = \frac{p_x}{(2 + L_2)} \left( \frac{y^3}{6} - \frac{y}{6} \right) + \frac{k\pi}{2}(y + 1) - \omega\pi \quad \text{for } y \in [-1, 0).$$

564 We now compute the inner solution. Substituting the inner variable (4.9) into  
565 (4.8a) and (4.8b), they become

$$566 \quad L^* S_{yy} + \dot{I}\dot{S} = 4L^*(S + IS) \left( \Theta_y + \frac{I\dot{\Theta}}{\sqrt{L^*}} \right)^2 + (S + IS)((S + IS)^2 - 1),$$

$$567 \quad (S + IS)(L^* \Theta_{yy} + \dot{I}\dot{\Theta}) = \frac{L^*}{2}(S + IS)u_y(\lambda\sqrt{L^*}) - 2L^* \left( S_y + \frac{I\dot{S}}{\sqrt{L^*}} \right) \left( \Theta_y + \frac{I\dot{\Theta}}{\sqrt{L^*}} \right),$$

568 where  $\dot{}$  denotes differentiation w.r.t  $\lambda$ . Letting  $L^* \rightarrow 0$ , we have that the leading  
569 order equations are

$$570 \quad (4.19a) \quad \dot{I}\dot{S} = 4(S + IS)(I\dot{\Theta})^2 + (S + IS)((S + IS)^2 - 1),$$

$$571 \quad (4.19b) \quad (S + IS)I\dot{\Theta} = -2I\dot{S}I\dot{\Theta},$$

573 or equivalently, after recalling  $S = 1$ ,

$$574 \quad \ddot{I}S = 2IS + q_1(IS, I\dot{\Theta}), \quad \ddot{I}\Theta = q_2(IS, I\dot{S}, I\dot{\Theta}, I\ddot{\Theta}),$$

575 where  $q_1, q_2$  represent the nonlinear terms of the equation. The linearised system is

$$576 \quad (4.20a) \quad \dot{I}S = 2IS,$$

$$577 \quad (4.20b) \quad \dot{I}\Theta = 0,$$

579 subject to the boundary and matching conditions

$$580 \quad (4.21a) \quad \lim_{\lambda \rightarrow \pm\infty} IS(\lambda) = 0, \quad IS(0) = s_{min} - 1,$$

$$581 \quad (4.21b) \quad \lim_{\lambda \rightarrow \pm\infty} I\Theta(\lambda) = 0,$$

583 where  $s_{min} \in [0, 1]$ , is the minimum value of  $s$ . We note that the second condition in  
584 (4.21a) ensures  $s(0) = s_{min}$ . Using the conditions (4.21a), the solution of (4.20a) is

$$585 \quad (4.22) \quad s(y) = \begin{cases} 1 + (s_{min} - 1)e^{-\sqrt{2}\frac{y}{\sqrt{L^*}}} & \text{for } 0 \leq y \leq 1 \\ 1 + (s_{min} - 1)e^{\sqrt{2}\frac{y}{\sqrt{L^*}}} & \text{for } -1 \leq y \leq 0. \end{cases}$$

586 With  $IS$  determined, we calculate  $I\Theta$ . Solving (4.20b) subject to the limiting condi-  
587 tions (4.21b), it is clear that  $I\Theta = 0$ . Hence,

$$588 \quad (4.23) \quad \theta(y) = \begin{cases} \frac{p_x}{(2+L_2)} \left( \frac{y^3}{6} - \frac{y}{6} \right) + \frac{k\pi}{2}(y-1) + \omega\pi & \text{for } 0 < y \leq 1 \\ \frac{p_x}{(2+L_2)} \left( \frac{y^3}{6} - \frac{y}{6} \right) + \frac{k\pi}{2}(y+1) - \omega\pi & \text{for } -1 \leq y < 0. \end{cases}$$

590 The expressions, (4.22) and (4.23), are consistent with our definition of an OR-type  
591 solution.

592 **4.2. Asymptotics for OR-type solutions in active nematodynamics, in**  
593 **the  $L^* \rightarrow 0$  limit.** Next, we consider an active nematic system in a channel geom-  
594 etry, i.e., a system that is constantly driven out of equilibrium by internal stresses  
595 and activity [20]. There are three dependent variables to solve for: the concentra-  
596 tion,  $c$ , of active particles, the fluid velocity  $\mathbf{u}$ , and the nematic order parameter  $\mathbf{Q}$ .  
597 The corresponding evolution equations are taken from [18, 17], with additional *active*  
598 *stresses* from the self-propelled motion of the active particles and the non-equilibrium  
599 intrinsic activity:

$$600 \quad (4.24a) \quad \frac{Dc}{Dt} = \nabla \cdot (\mathbf{D}\nabla c + \alpha_1 c^2 (\nabla \cdot \mathbf{Q})),$$

$$601 \quad (4.24b) \quad \nabla \cdot \mathbf{u} = 0, \quad \rho \frac{D\mathbf{u}}{Dt} = -\nabla p + \nabla \cdot (\mu(\nabla \mathbf{u} + (\nabla \mathbf{u})^T) + \tilde{\sigma}),$$

$$602 \quad (4.24c) \quad \frac{D\mathbf{Q}}{Dt} = \lambda s \mathbf{W} + \zeta \mathbf{Q} - \mathbf{Q}\zeta + \frac{1}{\gamma} \mathbf{H},$$

604 where  $\mathbf{W}$  is the symmetric part of the velocity gradient tensor,  $D_{ij} = D_0\delta_{ij} + D_1Q_{ij}$   
605 is the anisotropic diffusion tensor ( $D_0 = (D_{\parallel} + D_{\perp})/2$ ,  $D_1 = D_{\parallel} - D_{\perp}$  and  $D_{\parallel}$  and  $D_{\perp}$   
606 are, respectively, the bare diffusion coefficients along the parallel and perpendicular  
607 directions of the director field),  $\alpha_1$  is an activity parameter, and  $\lambda$  is the nematic  
608 alignment parameter, which characterizes the relative dominance of the strain and

609 the vorticity in affecting the alignment of particles with the flow [14]. For  $|\lambda| < 1$ , the  
 610 rotational part of the flow dominates, while for  $|\lambda| > 1$ , the director will tend to align  
 611 at a unique angle to the flow direction [15]. The value of  $\lambda$  is also determined by the  
 612 shape of the active particles [19]. The stress tensor,  $\tilde{\sigma} = \sigma^e + \sigma^a$  [21], is the sum of  
 613 an elastic stress due to nematic elasticity

$$614 \quad (4.25) \quad \sigma^e = -\lambda s \mathbf{H} + \mathbf{Q} \mathbf{H} - \mathbf{H} \mathbf{Q},$$

615 and an active stress defined by

$$616 \quad (4.26) \quad \sigma^a = \alpha_2 c^2 \mathbf{Q}.$$

617 Here  $\alpha_2$  is a second activity parameter, which describes extensile (contractile) stresses  
 618 exerted by the active particles when  $\alpha_2 < 0$  ( $\alpha_2 > 0$ ).  $\mathbf{H}$ ,  $\mu$ ,  $\xi$ ,  $p$  and  $\rho$ , are as  
 619 introduced in Section 2.

620 We again consider a one-dimensional static problem, with a unidirectional flow  
 621 in the  $x$  direction and take  $\lambda = 0$ . Then the evolution equations for  $\mathbf{Q}$  are the  
 622 same as those considered in the passive case, hence, making it easier to adapt the  
 623 calculations in section 4.1 and draw comparisons between the passive and active cases.  
 624 The isotropic to nematic phase transition is driven by the concentration of active  
 625 particles and as such, we take  $A = \kappa(c^* - c)/2$  and  $C = \kappa c$ , where  $c^* = \sqrt{3\pi/2L^2}$  is  
 626 the critical concentration at which this transition occurs [20, 18]. As in the passive  
 627 case, we work with  $A < 0$  i.e. with concentrations that favour nematic ordering.

628 The continuity equation (4.24a), follows from the fact that the total number of  
 629 active particles must remain constant [20]. This is compatible with constant concentra-  
 630 tion,  $c$ , although solutions with constant concentration do not exist for  $\alpha_1 \neq 0$ . We  
 631 consider the case of constant concentration  $c$ , which is not unreasonable for small val-  
 632 ues of  $\alpha_1$  and certain solution types (see supplementary material for further details),  
 633 and do not consider the concentration equation, (4.24a), in this work. We nondimen-  
 634 sionalise the system as before, but additionally scale  $c$  and  $c^*$  by  $L^{-2}$  (e.g.  $c = L^{-2}\tilde{c}$ ,  
 635 where  $\tilde{c}$  is dimensionless). In terms of  $\mathbf{Q}$ , the evolution equations are given by

$$636 \quad (4.27a) \quad \frac{\partial Q_{11}}{\partial t} = u_y Q_{12} + Q_{11,yy} + \frac{1}{L^*} Q_{11} (1 - 4(Q_{11}^2 + Q_{12}^2)),$$

$$637 \quad (4.27b) \quad \frac{\partial Q_{12}}{\partial t} = -u_y Q_{11} + Q_{12,yy} + \frac{1}{L^*} Q_{12} (1 - 4(Q_{11}^2 + Q_{12}^2)),$$

$$638 \quad (4.27c) \quad L_1 \frac{\partial u}{\partial t} = -p_x + u_{yy} + 2L_2 (Q_{11} Q_{12,yy} - Q_{12} Q_{11,yy})_y + \Gamma (Q_{12} c^2)_y,$$

640 where  $\Gamma = \frac{\alpha_2 \gamma}{\kappa \mu L^2} \sqrt{-\frac{2A}{C}}$  is a measure of activity. In the steady case, and in terms of  
 641  $(s, \theta)$ , the system (4.27) reduces to

$$642 \quad (4.28a) \quad s_{yy} = 4s\theta_y^2 + \frac{s}{L^*} (s^2 - 1),$$

$$643 \quad (4.28b) \quad s\theta_{yy} = \frac{1}{2} s u_y - 2s_y \theta_y,$$

$$644 \quad (4.28c) \quad u_{yy} = p_x - L_2 (s^2 \theta_y)_{yy} - \Gamma \left( \frac{c^2 s}{2} \sin(2\theta) \right)_y.$$

646 Regarding boundary conditions, we impose the same boundary conditions on  $s$ ,  $\theta$  and  
 647  $u$ , as in the passive case.

648 The equations, (4.28a) and (4.28b), are identical to the equations, (2.5a) and  
 649 (2.5b), respectively. Hence, the asymptotics in subsection 4.1 remain largely un-  
 650 changed, with differences coming from (4.28c), due to the additional active stress.  
 651 Skipping technical details which are analogous to those in Subsection 4.1, we find the  
 652 fluid velocity is given by

$$653 \quad (4.29) \quad u(y) = \int_{-1}^y \frac{2p_x Y - \Gamma c^2 s(Y) \sin(2\theta(Y))}{2g(s(Y))} dY.$$

654 Following methods in subsection 4.1, we pose asymptotic expansions as in (4.7a)  
 655 and (4.7b), for  $s$  and  $\theta$  respectively in the  $L^* \rightarrow 0$  limit, which yields (4.8a) and  
 656 (4.8b). In fact, the expression for  $s$  is given by (4.22), in the active case as well. For  
 657  $\Theta$ , we again solve (4.12) and find an implicit representation as given below:

$$658 \quad (4.30) \quad \Theta(y) = \begin{cases} \int_y^1 \frac{u(0)-u(Y)}{2} dY + \left( \frac{k\pi}{2} - \int_0^1 \frac{u(Y)-u(0)}{2} dY \right) (y-1) + \omega\pi, & 0 < y \leq 1 \\ \int_{-1}^y \frac{u(Y)-u(0)}{2} dY + \left( \frac{k\pi}{2} - \int_{-1}^0 \frac{u(Y)-u(0)}{2} dY \right) (y+1) - \omega\pi, & -1 \leq y < 0 \end{cases}$$

659 where  $u(y)$  is given by (4.29). Moving to the inner solution  $I\Theta$ , we need to solve  
 660 (4.20b), subject to the matching condition (4.21b). As before, we find  $I\Theta = 0$ , and  
 661 our composite expansion for  $\theta$  is just the outer solution presented above. We deduce  
 662 that OR-type solutions are still possible in an active setting, for the case  $\lambda = 0$ .

663 We now consider a simple case for which (4.30) can be solved explicitly. In (4.29),  
 664 we assume  $s = 1$  and  $\sin 2\theta = 1$  for  $-1 \leq y < 0$ , and  $\sin(2\theta) = -1$  for  $0 < y \leq 1$   
 665 i.e., we assume an OR solution with  $\theta = \mp \frac{\pi}{4}$  and  $\omega = -\frac{1}{4}$ . Under these assumptions,  
 666 (4.29) yields

$$667 \quad (4.31) \quad u(y) = \begin{cases} \frac{p_x}{2+L_2}(y^2-1) + \frac{\Gamma c^2}{2+L_2}(y-1), & \text{for } 0 < y \leq 1 \\ \frac{p_x}{2+L_2}(y^2-1) - \frac{\Gamma c^2}{2+L_2}(y+1), & \text{for } -1 \leq y < 0. \end{cases}$$

668 Substituting the above into (4.30), we find

$$669 \quad (4.32) \quad \theta(y) = \begin{cases} \frac{p_x}{2+L_2} \left( \frac{y^3}{6} - \frac{y}{6} \right) + \frac{\Gamma c^2}{2+L_2} \left( \frac{y^2}{4} - \frac{y}{4} \right) + \frac{k\pi}{2}(y-1) + \omega\pi, & \text{for } 0 < y \leq 1 \\ \frac{p_x}{2+L_2} \left( \frac{y^3}{6} - \frac{y}{6} \right) - \frac{\Gamma c^2}{2+L_2} \left( \frac{y^2}{4} + \frac{y}{4} \right) + \frac{k\pi}{2}(y+1) - \omega\pi & \text{for } -1 \leq y < 0. \end{cases}$$

670 We expect (4.31) and (4.32) to be good approximations to OR-type solutions with  
 671  $\omega = -\frac{1}{4}$ , in the limit of small  $\Gamma$  (small activity) and small pressure gradient, when  
 672 the outer solution is well approximated by an OR solution.

673 **4.3. Numerical results.** We solve the dynamical systems (2.4) and (4.27) with  
 674 finite element methods, and all simulations are performed using the open-source pack-  
 675 age FEniCS [28]. The details of the numerical methods are given in the supplementary  
 676 material. In the numerical results that follow, we extract the  $s$  profile from  $\mathbf{Q}$ , using  
 677 (2.3).

678 **4.3.1. Passive flows.** We begin by investigating whether OR-type solutions  
 679 exist for the passive system (2.4) when  $L^*$  is large (small  $\epsilon$ ), that is, for small nano-  
 680 scale channel domains. When  $\omega = \pm \frac{1}{4}$  and  $p_x = -1$ , we find profiles which are small  
 681 perturbations of the limiting OR solutions reported in the supplementary material,  
 682 for large  $L^*$  and  $p_x = 0$ , i.e., (2.7a), (2.7b) in the supplementary material when  
 683  $\omega = \pm \frac{1}{4}$  (see Fig. 3). We regard these profiles as being OR-type solutions although

684  $s(0) \neq 0$  but  $s(0) \ll 1$ , as the director profile resembles a polydomain structure and  $\theta$   
 685 jumps around  $y = 0$ , to satisfy its boundary conditions. As  $|p_x|$  increases, we lose this  
 686 approximate zero in  $s$ , i.e., we lose the domain wall and  $s \rightarrow 1$  almost everywhere.

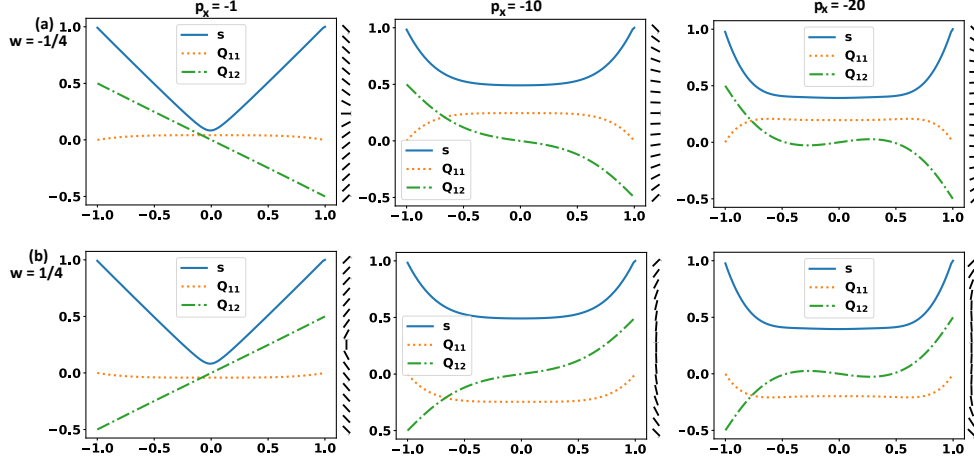


FIG. 3. The stable solutions of (2.4) for  $L^* = \infty$  (i.e., we remove the bulk contributions) and  $L_2 = 1e - 3$ . The values of  $p_x$  and  $\omega$ , are indicated in the plots (the same comments apply to all other figures where values are included in the plots).

687 We now proceed to study solutions of (2.4) in the  $L^* \rightarrow 0$  limit, relevant for  
 688 micron-scale channel domains. We study the stable equilibrium solutions, the ex-  
 689 istence of OR-type solutions in this limit, and how well the OR-type solutions are  
 690 approximated by the asymptotic expansions in Section 4.1. As expected, in Fig. 4  
 691 we find stable equilibria which satisfy  $s = 1$  almost everywhere and report unstable  
 692 OR-type solutions in Fig. 5, when  $\omega = -\frac{1}{4}$ . We again consider these to be OR-type  
 693 solutions despite  $s(0) \neq 0$ , since their behaviour is consistent with the asymptotic  
 694 expressions (4.22) and (4.23), and we also have approximate polydomain structures.  
 695 We also find these OR-type solutions for  $\omega = \frac{1}{4}$ , but do not report them as they are  
 696 similar to the  $\omega = -\frac{1}{4}$  case (the same is true in the next subsection). In fact,  $\omega = \pm\frac{1}{4}$   
 697 are the only boundary conditions for which we have been able to identify OR-type  
 698 solutions (identical comments apply to the active case).

699 In Fig. 5, we present three distinct OR-type solutions which vary in their  $Q_{11}$  and  
 700  $Q_{12}$  profiles, or equivalently the rotation of  $\theta$  between the bounding plates at  $y = \pm 1$ .  
 701 These numerical solutions are found by taking (4.22) (with  $s_{min} = 0$ ) and (4.23) with  
 702 different values of  $k$  ( $k = 0, 1, 2$ ), as the initial condition in our Newton solver. We  
 703 conjecture that one could build a hierarchy of OR-type solutions corresponding to  
 704 arbitrary integer values of  $k$  in (4.16), or different jumps in  $\theta$  at  $y = 0$  in (4.16),  
 705 when  $\omega = \pm\frac{1}{4}$ . OR-type solutions are unstable, and we speculate that the solutions  
 706 corresponding to different values of  $k$  in (4.16) are unstable equilibria with different  
 707 Morse indices, where the Morse index is a measure of the instability of an equilibrium  
 708 point [25]. A higher value of  $k$  could correspond to a higher Morse index or informally  
 709 speaking, a more unstable equilibrium point with more directions of instability. A  
 710 further relevant observation is that according to the asymptotic expansion (4.23),  
 711  $Q_{11}(0\pm) = 0$  and  $Q_{12}(0\pm) = \pm\frac{1}{2}$ , and hence the energy of the domain wall does  
 712 not depend strongly on  $k$ . The far-field behavior does depend on  $k$  in (4.23), and  
 713 we conjecture that this  $k$ -dependence generates the family of  $k$ -dependent OR-type

714 solutions. We note that OR-type solutions generally do not satisfy  $s(0) = 0$ , but  
 715  $s(0) \rightarrow 0$  as  $L^*$  decreases, for a fixed  $p_x$  (see Fig. 6).

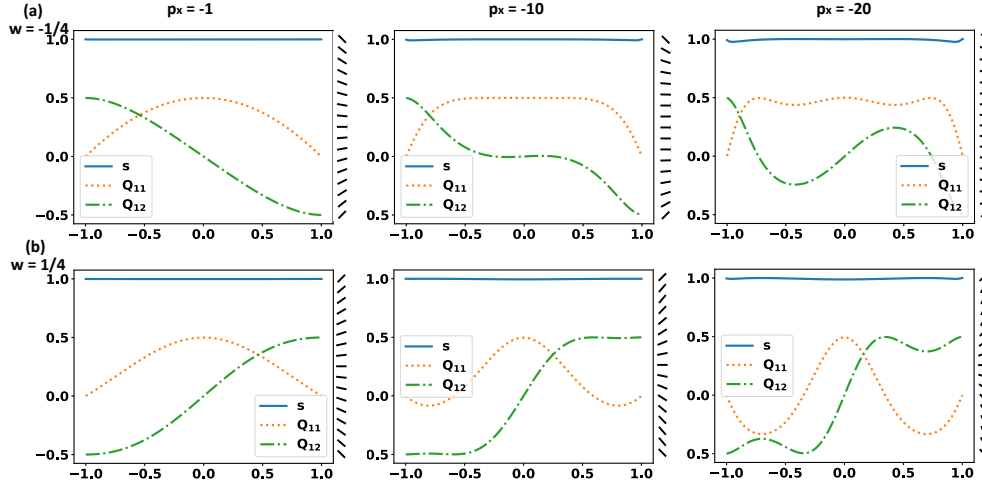


FIG. 4. Some example stable solutions of (2.4) for  $L^* = 1e - 3$  and  $L_2 = 1e - 3$ .

715

716

717

718

719

720

721

722

723

724

725

726

727

728

729

730

731

732

733

734

735

736

To conclude this section on passive flows, we assess the accuracy of our asymptotic  
 expansions in section 4.1. In Fig. 7, we plot the error between the asymptotic  
 expressions ((4.22) and (4.23)) and the corresponding numerical solutions of (2.4),  
 for the parameter values  $L^* = 1e - 4$ ,  $L_2 = 1e - 3$ ,  $p_x = -20$  and  $\omega = -\frac{1}{4}$ . More  
 precisely, we use these parameter values along with  $k = 1, 2, 3$  in (4.23), and (4.22)  
 with  $s_{min} = 0$ , to construct the asymptotic profiles. We then use these asymptotic  
 profiles as initial conditions to find the corresponding numerical solutions. Hence, we  
 have three comparison plots in Fig. 7, corresponding to  $k = 1, 2, 3$  respectively. By  
 error, we refer to the difference between the asymptotic profile and the corresponding  
 numerical solution. We label the asymptotic profiles using the superscript 0, in the  
 $L^* \rightarrow 0$  limit, whilst a nonzero superscript identifies the numerical solution along  
 with the value of  $L^*$  used in the numerics (these comments also apply to the active  
 case in the next section). We find good agreement between the asymptotics and  
 numerics, especially for the  $s$  profiles, where any error is confined to a narrow interval  
 around  $y = 0$  and does not exceed 0.07 in magnitude. Using (2.2), (4.22), and (4.23),  
 we construct the corresponding asymptotic profile  $\mathbf{Q}^0$ . Looking at the differences  
 between  $\mathbf{Q}^0$  and the numerical solutions  $\mathbf{Q}^{1e-4}$  (for  $k = 1, 2, 3$ ), the error does not  
 exceed 0.06 in magnitude. This implies good agreement between the asymptotic and  
 numerically computed  $\theta$ -profiles, at least for the parameter values under consideration.  
 While the fluid velocity  $u$  is not the focus of this work, we note that our asymptotic  
 profile (4.13), gives almost perfect agreement with the numerical solution for  $u$ .

737

738

739

740

741

742

743

**4.3.2. Active flows.** As explained previously, we consider active flows with  
 constant concentration  $c$ , and take  $c > c^*$ . To this end, we fix  $c = \sqrt{2\pi}$  in the  
 following numerical experiments. For  $L^*$  large (small nano-scale channel domains),  
 we find OR-type solutions when  $\omega = \pm\frac{1}{4}$ , and these are stable. In Fig. 8, we plot  
 these solutions when  $p_x = -1$  and for three different values of  $\Gamma$ , which we recall is  
 proportional to the activity parameter  $\alpha_2$ . We only have  $s(0) < 0.5$  when  $\Gamma = 1$ , in  
 which case the director profile exhibits polydomain structures. As  $\Gamma$  increases,  $s(0)$

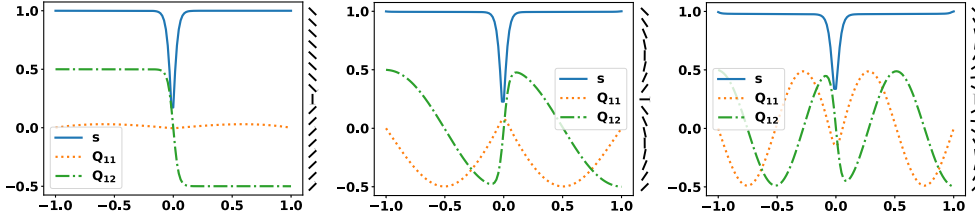


FIG. 5. Three unstable OR-type solutions (in the sense that they have transition layer profiles for  $s$ ) of (2.4) for  $L^* = 1e - 3$ ,  $L_2 = 1e - 3$ ,  $p_x = -1$  and  $\omega = -\frac{1}{4}$ . The initial conditions used are (4.22) (with  $s_{min} = 0$ ) and (4.23) with  $k = 0, 1, 2$  (from left to right), along with the parameter values just stated.

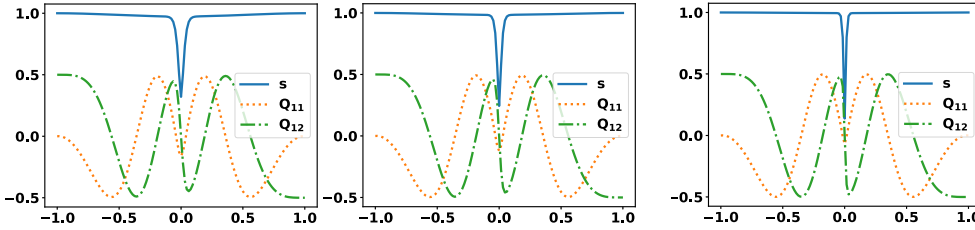


FIG. 6. Plot of an OR-type solution for  $L^* = 5e - 4$ ,  $3e - 4$ ,  $1e - 4$  (from left to right). The remaining parameter values are  $L_2 = 1e - 3$ ,  $p_x = -20$  and  $\omega = -\frac{1}{4}$ . The initial conditions used are (4.22) (with  $s_{min} = 0$ ) and (4.23) with  $k = 2$ , along with the parameter values just stated.

744 increases and  $s \rightarrow 1$  almost everywhere, so that OR-type solutions are only possible  
 745 for small values of  $p_x$  and  $\Gamma$ . Increasing  $|p_x|$  for a fixed value of  $\Gamma$ , also drives  $s \rightarrow 1$   
 746 everywhere.

747 As in the passive case, we also find unstable OR-type solutions consistent with  
 748 the limiting asymptotic expression (4.22), for small values of  $L^*$  that correspond to  
 749 micron-scale channels. The stable solutions have  $s \approx 1$  almost everywhere (see Fig.  
 750 9). In Fig. 10, we find unstable OR-type solutions when  $L^* = 1e - 3$ ,  $L_2 = 1e - 3$  and  
 751  $\omega = -\frac{1}{4}$ , for a range of values of  $p_x$  and  $\Gamma$ . To numerically compute these solutions,  
 752 we use the stated parameter values in (4.22) (with  $s_{min} = 0$ ) and (4.32), along with  
 753  $k = 0$ , as our initial condition. We only have  $s(0) \approx 0$  provided  $|p_x|$  and  $\Gamma$  are not  
 754 too large, however,  $s(0) \rightarrow 0$  in the  $L^* \rightarrow 0$  limit for fixed values of  $p_x$  and  $\Gamma$ . This  
 755 illustrates the robustness of OR-type solutions in an active setting. In Fig. 11, we plot  
 756 three further distinct OR-type solutions, obtained by taking (4.22) (with  $s_{min} = 0$ )  
 757 and (4.32) with  $k = 1, 2, 3$ , as our initial condition. Hence, for the same reasons as  
 758 in the passive case, we believe there may be multiple unstable OR-type solutions,  
 759 corresponding to different values of  $k$  in (4.16).

760 By analogy with the passive case, we now compare the asymptotic expressions  
 761 (4.22), (4.31) and (4.32), with the numerical solutions. The error plots are given in  
 762 Fig. 12. Once again, there is good agreement between the limiting  $s$ -profile (4.22) and  
 763 the numerical solutions, where any error is confined to a small interval around  $y = 0$ .  
 764 There is also good agreement between the asymptotic and numerically computed  $\theta$ -  
 765 profiles (coded in terms of  $Q_{11}$  and  $Q_{12}$ ) and flow profile  $u$ , provided  $|p_x|$ ,  $\Gamma$ , or both,  
 766 are not too large. When  $|p_x|$  and  $\Gamma$  are large (say much greater than 1), the accuracy of  
 767 the asymptotics breaks down, especially for the  $u$ -profile. However, OR-type solutions

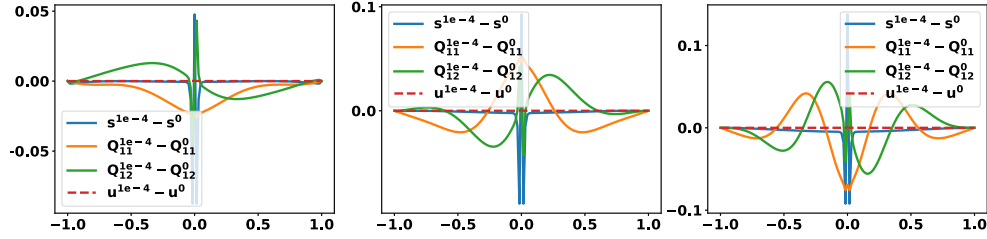


FIG. 7. Plot of  $\mathbf{Q}^{1e-4} - \mathbf{Q}^0$ ,  $s^{1e-4} - s^0$ , and  $u^{1e-4} - u^0$ . Here,  $\mathbf{Q}^0$  is the asymptotic profile given by (4.22) and (4.23) with,  $s_{min} = 0$ ,  $k = 1, 2, 3$  (from left to right),  $L^* = 1e-4$ ,  $L_2 = 1e-3$ ,  $p_x = -20$  and  $\omega = -1/4$ , whilst  $\mathbf{Q}^{1e-4}$  denotes the corresponding numerical solution of (2.4).  $s^0$  is given by (4.22) and  $s^{1e-4}$  is extracted from  $\mathbf{Q}^{1e-4}$ . The numerical solutions are found by using  $\mathbf{Q}^0$  as the initial condition. Identical comments apply to  $u^0 - u^{1e-4}$ , where  $u^0$  is given by (4.13) and  $u^{1e-4}$  is the numerical solution of (2.4).

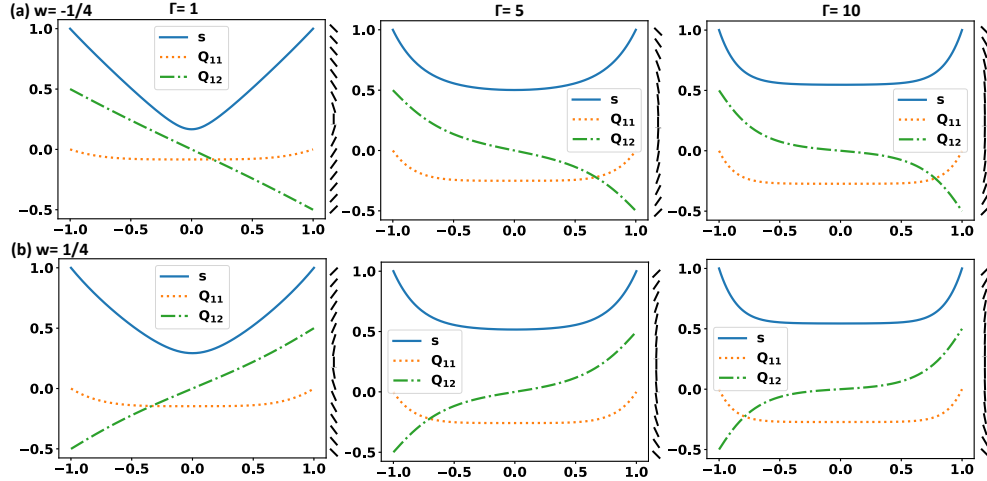


FIG. 8. The stable solutions of (4.27) for  $L^* = \infty$ ,  $L_2 = 1e-3$ ,  $c = \sqrt{2\pi}$  and  $p_x = -1$ .

768 are still possible for large values of  $|p_x|$  and  $\Gamma$ , as elucidated by Fig. 10.

769 **5. Conclusions.** In this article, we have demonstrated the universality of OR-  
 770 type solutions in NLC-filled microfluidic channels. Section 3 focuses on the simple  
 771 and idealised case of constant flow and pressure to give some preliminary insight into  
 772 the more complex systems considered in section 4. We prove a series of results that  
 773 lead to the interesting and non-obvious conclusion, that the multiplicity of observable  
 774 equilibria depends on the boundary conditions. We employ an  $(s, \theta)$ -formalism for the  
 775 NLC state, and impose Dirichlet conditions for  $(s, \theta)$  coded in terms of  $\omega$ , where  $\omega$   
 776 is a measure of the director rotation between the bounding plates  $y = \pm 1$ . We always  
 777 have a unique smooth solution in this framework, provided an OR solution does not  
 778 exist (Theorem 3.4). Additionally, in the  $\mathbf{Q}$ -framework for  $\omega = \pm \frac{1}{4}$ , i.e., when the  
 779 boundary conditions are orthogonal to each other, OR solutions with polydomain  
 780 structures exist for all values of  $L^*$  or  $\epsilon$ , they are globally stable for large  $L^*$  (small  
 781  $\epsilon$ ), and there are multiple solutions for small values of  $L^*$  (large  $\epsilon$ ) or large channel  
 782 geometries. In fact, for all three scenarios considered in this paper, we have found OR  
 783 and OR-type solutions to be compatible with  $\omega = \pm \frac{1}{4}$  only, or orthogonal boundary

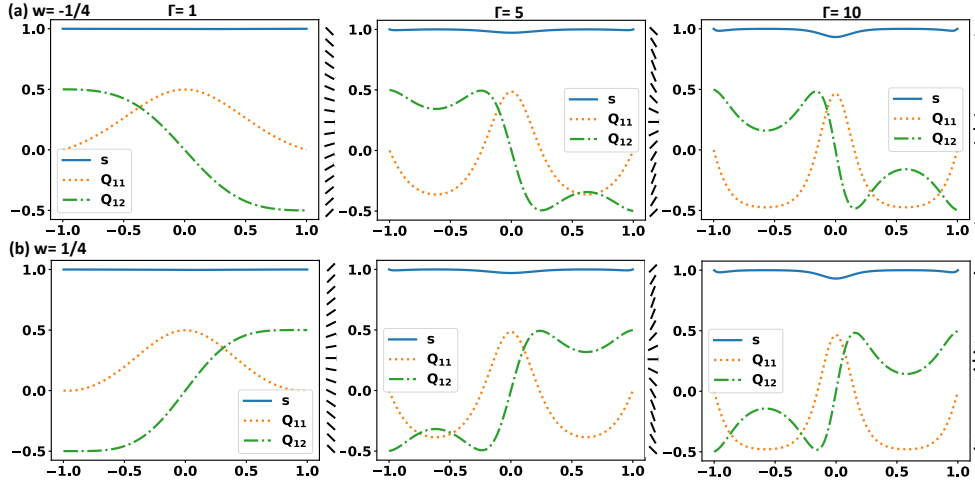


FIG. 9. The stable solutions of (4.27) for  $L^* = 1e - 3$ ,  $L_2 = 1e - 3$ ,  $c = \sqrt{2\pi}$  and  $p_x = -1$ .

784 conditions. We note that in Theorem 7 of [3], the author proves that minimizers of  
 785 an Oseen-Frank energy in three dimensions are unique for non-orthogonal boundary  
 786 conditions. This result is clearly different from ours, based on different arguments, but  
 787 has a similar physical flavour. As has been noted in [2] amongst others, orthogonal  
 788 boundary conditions allow for solutions in the  $\mathbf{Q}$ -formalism (solutions of (3.1)) that  
 789 have a constant set of eigenvectors in space. These solutions, with a constant set of  
 790 eigenvectors, are precisely the OR solutions, which are disallowed for non-orthogonal  
 791 boundary conditions. Thus, whilst the conclusion of Theorem 3.1 is not surprising,  
 792 we recover the same result with different arguments in the  $(s, \theta)$ -framework, which is  
 793 of independent interest.

794 In section 4, we calculate useful asymptotic expansions for OR-type solutions in  
 795 the limit of large domains, for both passive and active nematics. The asymptotics are  
 796 validated by numerically-computed OR-type solutions for small and large values of  
 797  $L^*$ , using the asymptotic expansions as initial conditions. There is good agreement  
 798 between the asymptotics and the numerical solutions, and the asymptotics give good  
 799 insight into the internal structure of domain walls of OR-type solutions and the outer  
 800 far-field solutions. These techniques can be further embellished to include external  
 801 fields, other types of boundary conditions, and more complex geometries as well.

802 In section 4.3, the OR-type solutions are unstable for small  $L^*$  or large channels.  
 803 However, they may still be observable and hence, physically relevant. In the exper-  
 804 imental results in [1] for passive NLC-filled microfluidic channels, the authors find  
 805 disclination lines at the centre of a microfluidic channel filled with the liquid crystal  
 806 5CB, with flow, both with and without an applied electric field. Moreover, the au-  
 807 thors are able to stabilise these disclination lines by applying an electric field. So,  
 808 while the OR-type solutions are unstable mathematically, they can be stabilised or  
 809 controlled/exploited for transport phenomena and cargo transport in experiments. In  
 810 the active case, there are similar experimental results in [23]. Here the authors apply  
 811 a magnetic field to 8CB in the smectic-A phase placed on top of an aqueous gel of  
 812 microtubules cross-linked by ATP-activated kinesin motor clusters (constituting the  
 813 active nematic system), and observe the formation of parallel lanes of defect cores in  
 814 the active nematic, aligned perpendicularly to the magnetic field. These defect cores

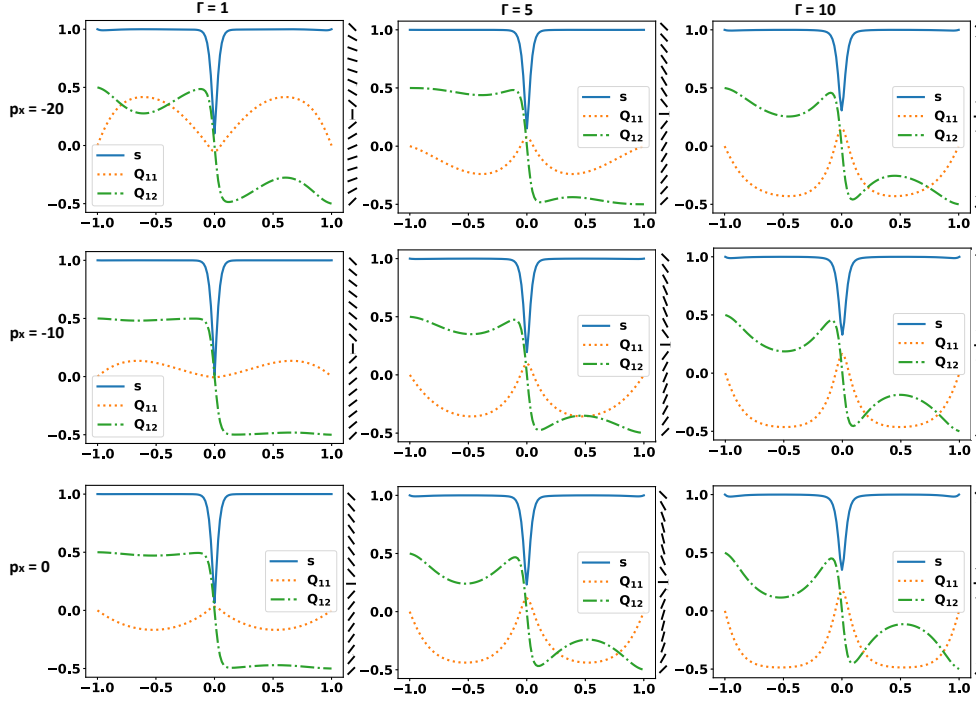


FIG. 10. Unstable OR-type solutions (in the sense that they have transition layer profiles for  $s$ ) of (4.27), for  $L^* = 1e-3$ ,  $L_2 = 1e-3$ ,  $c = \sqrt{2\pi}$  and  $\omega = -\frac{1}{4}$ . The initial conditions used are (4.22) (with  $s_{min} = 0$ ) and (4.32) with  $k = 0$ .

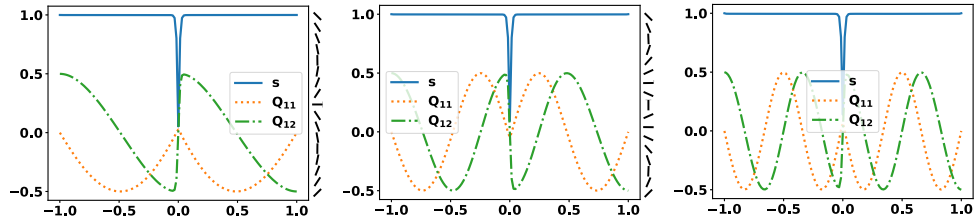


FIG. 11. Three unstable OR-type solutions of (4.27) for  $L^* = 1e-3$ ,  $L_2 = 1e-3$ ,  $p_x = -1$ ,  $\Gamma = 0.7$  and  $\omega = -\frac{1}{4}$ .

815 and disclination lines can be modelled by OR-type solutions, as we have studied in  
 816 this paper. In general, we argue that unstable solutions are of independent interest  
 817 since they play crucial roles in the connectivity of solution landscapes of complex  
 818 systems [25]. Unstable solutions steer the dynamics of a system and dictate the selec-  
 819 tion of the steady state for multistable systems (with multiple stable states). Hence,  
 820 OR-type solutions are unstable for large domains, but can influence non-equilibrium  
 821 properties or perhaps be stabilised for tailor-made applications.

822 To conclude this article, we argue why OR-type solutions maybe universal in  
 823 variational theories, with free energies that employ a Dirichlet elastic energy for the  
 824 unknowns, e.g.  $y_1 \dots y_n$  for  $n \in \mathbb{N}$ . Working in a one-dimensional setting, consider an

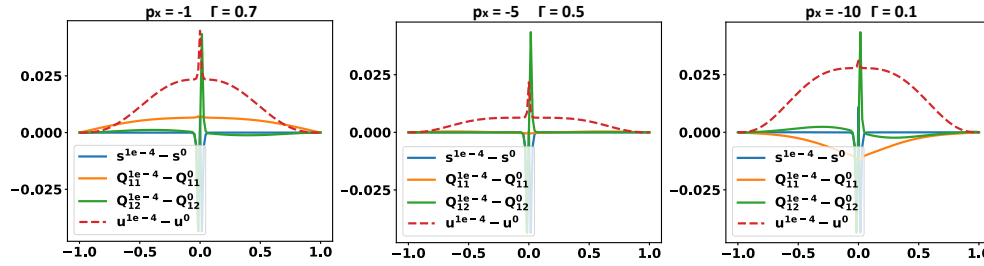


FIG. 12. Plot of  $\mathbf{Q}^{1e-4} - \mathbf{Q}^0$ ,  $s^{1e-4} - s^0$ , and  $u^{1e-4} - u^0$ . Here,  $\mathbf{Q}^0$  is given by (4.22) and (4.32) with,  $s_{min} = 0$ ,  $k = 0$ ,  $c = \sqrt{2\pi}$ ,  $L^* = 1e-4$ ,  $L_2 = 1e-3$ ,  $p_x$  and  $\Gamma$  as stated in the figure, and  $\omega = -1/4$ , whilst  $\mathbf{Q}^{1e-4}$  is the numerical solution of (4.27), with the same parameter values.

825 energy of the form

$$826 \quad (5.1) \quad \int_{\Omega} y_1'(x)^2 + \dots y_n'(x)^2 + \frac{1}{L^*} h(y_1, \dots, y_n)(x) \, dx,$$

827 subject to Dirichlet boundary conditions, for a material-dependent positive elastic  
 828 constant  $L^*$ . The function,  $h$ , models a bulk energy that only depends on  $y_1, \dots, y_n$ .  
 829 As  $L^* \rightarrow \infty$ , the limiting Euler-Lagrange equations admit unique solutions of the  
 830 form  $y_j = ax + b$ , for constants  $a$  and  $b$ . For specific choices of  $\Omega$  and asymmetric  
 831 boundary conditions, we can have domain walls at  $x = x^*$  such that  $y_j(x^*) = 0$  for  
 832  $j = 1, \dots, n$ . Writing each  $y_j = |y_j| \text{sgn}(y_j)$ , the domain wall separates polydomains  
 833 with phases differentiated by different values of  $\text{sgn}(y_j)$ . Moreover, we believe this  
 834 argument can be extended to systems in two and three-dimensions.

835 **Acknowledgments.** We thank Giacomo Canevari for helpful comments on some  
 836 of the proofs in Section 3.

837 **Taxonomy.** The author names are listed alphabetically. JD led the project,  
 838 which was conceived and designed by AM and LM. YH produced all the numerics  
 839 and contributed to the analysis. JD, AM and LM wrote the manuscript carefully and  
 840 oversaw the project evolution. AM mentored JD and YH throughout the project.

841

## REFERENCES

- 842 [1] H. AGHA AND C. BAHR, *Nematic line defects in microfluidic channels: wedge, twist and zigzag*  
 843 *disclinations*, *Soft Matter*, 14 (2018), pp. 653–664.  
 844 [2] L. AMBROSIO AND E. G. VIRGA, *A boundary-value problem for nematic liquid crystals with a*  
 845 *variable degree of orientation*, *Arch. Ration. Mech. Anal.*, 114 (1991), pp. 335–347.  
 846 [3] J. BALL, *Mathematics and liquid crystals*, *Mol. Cryst. Liq. Cryst.*, 647 (2017), pp. 1–27.  
 847 [4] A. N. BERIS AND B. J. EDWARDS, *Thermodynamics of Flowing Systems: With Internal Mi-*  
 848 *crostructure*, Oxford University Press, Oxford, UK, 1994.  
 849 [5] F. BETHUEL, H. BREZIS, AND F. HÉLEIN, *Asymptotics for the minimization of a Ginzburg–*  
 850 *Landau functional*, *Calc. Var. Partial Diff.*, 1 (1993), pp. 123–148.  
 851 [6] A. BRAIDES, *A handbook of  $\Gamma$ -convergence*, in *Handbook of Differential Equations: Stationary*  
 852 *Partial Differential Equations*, vol. 3, Elsevier, North-Holland, Amsterdam, 2006, pp. 101–  
 853 213.  
 854 [7] M. CALDERER AND B. MUKHERJEE, *Chevron patterns in liquid crystal flows*, *Physica D: Non-*  
 855 *linear Phenomena*, 98 (1996), p. 201–224.  
 856 [8] G. CANEVARI, J. HARRIS, A. MAJUMDAR, AND Y. WANG, *The well order reconstruction solution*  
 857 *for three-dimensional wells, in the Landau–de Gennes theory*, *Int. J. Non-Linear Mech.*,  
 858 119 (2020), p. 103342.  
 859 [9] G. CANEVARI, A. MAJUMDAR, AND A. SPICER, *Order reconstruction for nematics on squares*  
 860 *and hexagons: a Landau–de Gennes study*, *SIAM J. Appl. Math.*, 77 (2019), pp. 267–293.

- 861 [10] S. ČOPAR, Ž. KOS, T. EMERŠIČ, AND U. TKALEC, *Microfluidic control over topological states*  
862 *in channel-confined nematic flows*, Nat. Commun., 11 (2020), pp. 1–10.
- 863 [11] J. CUENNET, A. E. VASDEKIS, AND D. PSALTIS, *Optofluidic-tunable color filters and spectroscopy*  
864 *based on liquid-crystal microflows*, Lab on a Chip, 13 (2013), pp. 2721–2726.
- 865 [12] J. DALBY, P. FARRELL, A. MAJUMDAR, AND J. XIA, *One-Dimensional Ferronematics in a*  
866 *Channel: Order Reconstruction, Bifurcations and Multistability*, SIAM J. on Appl. Math.,  
867 82 (2022), pp. 694–719.
- 868 [13] P. G. DE GENNES, *The Physics of Liquid Crystals*, Oxford University Press, Oxford, 1974.
- 869 [14] A. DOOSTMOHAMMADI, J. IGNÉS-MULLOL, J. M. YEOMANS, AND F. SAGUÉS, *Active nematics*,  
870 Nat. Commun., 9 (2018), p. 3246.
- 871 [15] S. A. EDWARDS AND J. M. YEOMANS, *Spontaneous flow states in active nematics: A unified*  
872 *picture*, Europhysics letters, 85 (2005), p. 18008.
- 873 [16] L. FANG, A. MAJUMDAR, AND L. ZHANG, *Surface, size and topological effects for some nematic*  
874 *equilibria on rectangular domains*, Math. Mech. Solids, 25 (2020), pp. 1101–1123.
- 875 [17] L. GIOMI, M. BOWICK, X. MA, AND M. MARCHETTI, *Defect annihilation and proliferation in*  
876 *active nematics*, Phys. Rev. Lett., 110 (2013), pp. 228101–1–228101–5.
- 877 [18] L. GIOMI, M. BOWICK, P. MISHRA, R. SKNEPNEK, AND M. MARCHETTI, *Defect dynamics in*  
878 *active nematics*, Phil. Trans. R.Soc. A, 372 (2014), p. 20130365.
- 879 [19] L. GIOMI, T. B. LIVERPOOL, AND M. MARCHETTI, *Sheared active fluids: Thickening, thinning,*  
880 *and vanishing viscosity*, Phys. Rev. E, 81 (2010), p. 051908.
- 881 [20] L. GIOMI, L. MAHADEVAN, B. CHAKRABORTY, AND M. HAGAN, *Banding, excitability and chaos*  
882 *in active nematic suspensions*, Nonlinearity, 25 (2012), p. 2245–2269.
- 883 [21] L. GIOMI, L. MAHADEVAN, B. CHAKRABORTY, AND M. F. HAGAN, *Excitable patterns in active*  
884 *nematics*, Phys. Rev. L., 106 (2011), p. 218101.
- 885 [22] D. GOLOVATY, J. MONTERO, AND P. STERNBERG, *Dimension Reduction for the Landau-de*  
886 *Gennes Model in Planar Nematic Thin Films*, J. Nonlinear Sci., 25 (2015), pp. 1431–1451.
- 887 [23] P. GUILLAMAT, J. IGNÉS-MULLOL, AND F. SAGUÉS, *Control of active liquid crystals with a*  
888 *magnetic field*, Proc. Natl. Acad. Scis, 113 (2016), pp. 5498–5502.
- 889 [24] Y. HAN, A. MAJUMDAR, AND L. ZHANG, *A reduced study for nematic equilibria on two-*  
890 *dimensional polygons*, SIAM J. Appl. Math., 80 (2020), pp. 1678–1703.
- 891 [25] Y. HAN, J. YIN, P. ZHANG, A. MAJUMDAR, AND L. ZHANG, *Solution landscape of a reduced*  
892 *landau-de gennes model on a hexagon*, Nonlinearity, 34 (2021), pp. 2048–2069.
- 893 [26] X. LAMY, *Bifurcation analysis in a frustrated nematic cell*, J. Nonlinear Sci., 24 (2014),  
894 pp. 1197–1230.
- 895 [27] A. H. LEWIS, I. GARLEA, J. ALVARADO, O. J. DAMMONE, P. D. HOWELL, A. MAJUMDAR, B. M.  
896 MULDER, M. LETTINGA, G. H. KOENDERINK, AND D. G. AARTS, *Colloidal liquid crystals*  
897 *in rectangular confinement: Theory and experiment*, Soft Matter, 10 (2014), p. 7865–7873.
- 898 [28] A. LOGG, K.-A. MARDAL, AND G. WELLS, *Automated solution of differential equations by the*  
899 *finite element method: The FEniCS book*, vol. 84, Springer Science & Business Media,  
900 2012.
- 901 [29] A. MAJUMDAR, *Equilibrium order parameters of nematic liquid crystals in the Landau-de*  
902 *Gennes theory*, Euro. J. Appl. Math, 21 (2010), pp. 181–203.
- 903 [30] M. C. MARCHETTI, J.-F. JOANNY, S. RAMASWAMY, T. B. LIVERPOOL, J. PROST, M. RAO, AND  
904 R. A. SIMHA, *Hydrodynamics of soft active matter*, Rev. Mod. Phys., 85 (2013), p. 1143.
- 905 [31] S. MONDAL, I. GRIFFITHS, F. CHARLET, AND A. MAJUMDAR, *Flow and nematic director pro-*  
906 *files in a microfluidic channel: the interplay of nematic material constants and backflow*,  
907 Fluids, 3 (2018), p. 39.
- 908 [32] L. MRAD AND D. PHILLIPS, *Dynamic analysis of chevron structures in liquid crystal cells*, Mol.  
909 Cryst. Liq. Cryst., 647 (2017), pp. 66–91.
- 910 [33] T. P. RIEKER, N. A. CLARK, G. S. SMITH, D. S. PARMAR, E. B. SIROTA, AND C. R. SAFINYA,  
911 “chevron” local layer structure in surface-stabilized ferroelectric smectic-c cells, Phys. Rev.  
912 Lett., 59 (1987), pp. 2658–2661.
- 913 [34] N. SCHOPHL AND T. J. SLUCKIN, *Defect Core Structure in Nematic Liquid Crystals*, Phys.  
914 Rev. Lett., 59 (1987), pp. 2582–2584.
- 915 [35] A. SENGUPTA, C. BAHR, AND S. HERMINGHAUS, *Topological microfluidics for flexible micro-*  
916 *cargo concepts*, Soft Matter, 9 (2013), pp. 7251–7260.
- 917 [36] C. TSAKONAS, A. J. DAVIDSON, C. V. BROWN, AND N. J. MOTTRAM, *Multistable alignment*  
918 *states in nematic liquid crystal filled wells*, Applied physics letters, 90 (2007), p. 111913.
- 919 [37] Y. WANG, G. CANEVARI, AND A. MAJUMDAR, *Order reconstruction for nematics on squares*  
920 *with isotropic inclusions: a Landau-de Gennes study*, SIAM J. Appl. Math., 79 (2019),  
921 pp. 1314–1340.